UPPSALA
UNIVERSITET

Digital Comprehensive Summaries of Uppsala Dissertations from the Faculty of Science and Technology 706

Proton-Coupled Electron Transfer from Hydrogen-Bonded Phenols

TANIA IREBO

ACTA
UNIVERSITATIS
UPSALIENSIS
UPPSALA
2010

ISSN 1651-6214
ISBN 978-91-554-7699-1
urn:nbn:se:uu:diva-112060

Dissertation presented at Uppsala University to be publicly examined in Häggsalen, Ångströmslaboratoriet, Lägerhyddsvägen 1, Uppsala, Friday, February 19, 2010 at 10:15 for the degree of Doctor of Philosophy. The examination will be conducted in English.

Abstract
Irebo, T. 2010. Proton-Coupled Electron Transfer from Hydrogen-Bonded Phenols. Acta Universitatis Upsaliensis. *Digital Comprehensive Summaries of Uppsala Dissertations from the Faculty of Science and Technology* 706. 68 pp. Uppsala. ISBN 978-91-554-7699-1.

Proton-coupled electron transfer (PCET) is one of the elementary reactions occurring in many chemical and biological systems, such as photosystem II where the oxidation of tyrosine (Tyr_Z) is coupled to deprotonation of the phenolic proton. This reaction is here modelled by the oxidation of a phenol covalently linked to a $Ru(bpy)_3^{2+}$-moitey, which is photo-oxidized by a laser flash-quench method. This model system is unusual as mechanism of PCET is studied in a unimolecular system in water solution. Here we address the question how the nature of the proton accepting base and its hydrogen bond to phenol influence the PCET reaction.

In the first part we investigate the effect of an internal hydrogen bond PCET from. Two similar phenols are compared. For both these the proton accepting base is a carboxylate group linked to the phenol on the ortho-position directly or via a methylene group. On the basis of kinetic and thermodynamic arguments it is suggested that the PCET from these occurs via a concerted electron proton transfer (CEP). Moreover, numerical modelling of the kinetic data provides an in-depth analysis of this CEP reaction, including promoting vibrations along the O–H–O coordinate that are required to explain the data.

The second part describes the study on oxidation of phenol where either water or an external base the proton acceptor. The pH-dependence of the kinetics reveals four mechanistic regions for PCET within the same molecule when water is the base. It is shown that the competition between the mechanisms can be tuned by the strength of the oxidant. Moreover, these studies reveal the conditions that may favour a buffer-assisted PCET over that with deprotonation to water solution.

Keywords: Proton-coupled electron transfer, phenol oxidation, hydrogen bonds, artificial photosynthesis, promoting vibrations, proton transfer, laser flash-quench, transient absorption.

Tania Irebo, Department of Photochemistry and Molecular Science, Chemical Physics, Box 523, Uppsala University, SE-75120 Uppsala, Sweden

ISSN 1651-6214
ISBN 978-91-554-7699-1
urn:nbn:se:uu:diva-112060 (http://urn.kb.se/resolve?urn=urn:nbn:se:uu:diva-112060)

List of Papers

This thesis is based on the following papers, which are referred to in the text by their Roman numerals.

I **Kinetic Effects of Hydrogen Bonds on Proton-Coupled Electron Transfer from Phenols**
M. Sjödin, T. Irebo, J. E. Utas, J. Lind, G. Merenyi, B. Åkermark, L. Hammarström
Journal of the American Chemical Society **2006**, *128*, 13076.

II **Proton-Coupled Electron Transfer of Tyrosine Oxidation: Buffer Dependence and Parallel Mechanisms**
T. Irebo, S. Y. Reece, M. Sjödin, D. G. Nocera, L. Hammarström
Journal of the American Chemical Society **2007**, *129*, 15462.

III **The Rate Ladder of Proton-Coupled Tyrosine Oxidation in Water: A Systematic Dependence on Hydrogen Bonds and Protonation State**
T. Irebo, O. Johansson, L. Hammarström
Journal of the American Chemical Society **2008**, *130*, 9194.

IV **The Kinetic Effect of Internal Hydrogen Bonds on Proton-Coupled Electron Transfer from Phenols: A Theoretical Analysis with Modeling of Experimental Data**
L. O. Johannissen, T. Irebo, M. Sjödin, O. Johansson, L. Hammarström
Journal of Physical Chemistry B **2009,** *113,* 16214.

V **Spanning Four Mechanistic Regions of Proton-Coupled Electron Transfer in a Single $Ru(bpy)_3^{2+}$-Tyrosine Complex**
T. Irebo, M. Zhang, A. Scott, L. Hammarström
Manuscript in progress

Contribution report

Paper **I** Contributed with the kinetic measurement and data analysis of the phenol oxidation.

Paper **II** Contributed with all measurements and data analysis for **RuY** and $\mathbf{Ru_{ester}Y}$. Contributions to the planning of experiments. Major contribution to the interpretation of the results and to the writing of the manuscript.

Paper **III** Contributed with all the kinetic measurements and the analysis of the data. Made major contribution to the interpretation of the results and planning of the experiments. Major contribution to the writing of the manuscript.

Paper **IV** Contributed with all experimental work. Contributed to the writing of the experimental parts of the manuscript.

Paper **V** Contributed with all of the measurements on **Ru-Y** and most of the measurement on $\mathbf{Ru_{me}}$**-Y**. Major contributions to formulation of the research problem and interpretation of the results. Minor contribution to the writing of the manuscript.

I have contributed to the discussions of all the papers above.

Contents

Abbreviations

$[Ru(bpy)_3]^{2+}$	ruthenium(II) trisbipyridine
ATP	adenosine triphosphate
CEP	concerted electron proton transfer
e^-	electron
$E°$	standard potential
$E°'$	formal potential
E_a	activation energy
ET	electron transfer
ETPT	stepwise electron proton transfer
F	Faraday constant
H^+	proton
H-bond	hydrogen bond
k_B	Boltzmann constant
KIE	kinetic isotope effect
NADPH	reduced nicotinamide adenine dinucleotide phosphate
PA	2-hydroxyphenylacetic acid derivate
PCET	proton-coupled electron Transfer
PhO^-	deprotonated phenol, phenolate
$PhO^\bullet$	phenol radical
PhOH	phenol
$PhOH^{\bullet+}$	phenol radical cation
PSII	photosystem II
PT	proton transfer
PTET	stepwise proton electron transfer
R	Gas constant
SA	salicylic acid derivate
T	temperature
$TyrO^-$	deprotonated tyrosine, tyrosinate
$TyrO^\bullet$	tyrosine radical
TyrOH	tyrosine
$TyrOH^{\bullet+}$	tyrosine radical cation
Y	tyrosine
$\Delta G^\#$	activation free energy
$\Delta G°$	standard free energy change
$\Delta G°'$	formal free energy change
λ	reorganization energy

1 Introduction

Two of the most elementary and widespread processes in chemistry and biology are proton transfer and electron transfer. Such processes are frequently found to be coupled in natural enzymes. One example is the oxidation of a tyrosine (Y_Z) in photosystem II. These reactions are of great interest and may be crucial in the development of *artificial photosynthesis.* The challenge there is to master these elementary processes in order to be able to produce high-energy chemical fuel using solar energy. With good model systems these processes can be studied in man-made molecules, designed to answer particular questions. This thesis describes the studies on the *proton-coupled electron transfer* (PCET) in phenols situated in model complexes. One of the questions addressed is the influence of hydrogen bonds on the PCET processes from phenols.

One of the first papers on proton-coupled electron transfer was published almost 30 years ago.[1] Since then, over 600 papers have been published on the same subject and over 50 % of these have occurred in the last five years. In other words, the interest of this process has recently been raised remarkably. This work is inspired by the oxidation of Y_Z in photosystem II, but PCET reactions are also found to be important in other biological systems. To cite a few examples, cytochrome oxidases[2,3], ribonucleotide reductase[4], DNA photolyase[5], anti-oxidant activity[6] and C-H activation[7,8]. This further confirms the importance to understanding the fundamentals of this chemical reaction step.

1.1 Background and perspective

The world faces an impending energy crisis as the global population is growing while our existing energy supplies are becoming scarce. Today the most dominant energy resources come from fossil fuels,[9] and there is no doubt that the combustion of these fuels have caused the emission of green-house gases. It has been heavily debated but is now more or less proven that the climate changes that we are facing, as the increase in global atmospheric CO_2 concentrations, rise in global average temperature and melting of the mountain glaciers, are really an effect from human activity.[10] The use of fossil fuels has not only an environmental impact, but these reserves are not limitless. The worldwide energy consumption is at present approaching 14 TW but is projected to be doubled by 2050.[11,12] Meeting the earth energy demand will require not only improved efficiency of the current technologies but also a new clean form of renewable energy source.

An important possibility lies in solar energy. There is more solar energy reaching the surface of the earth each hour than humans use over a whole year.[12] Clearly, it has the capacity of providing enough energy for the human civilization. The solar energy may either be converted to a fuel (like hydrogen), into thermal energy (heat) or into electricity. The latter is accomplished in photovoltaic modules. These produce high energy conversion efficiency but the current is only produced under active illumination. The materials of solar cells are still too expensive to cover the world-wide requirements. Scientific efforts are made to invent low cost solar cells, as dye-sensitized solar cells and organic solar cells but the challenge here is to make them efficient enough and at the same time long-term stable.[13,14]

In order for solar energy to be viable on large scale the energy must be stored for use during periods of low light. For example, excited state energy could be used to drive chemical reactions that produce high-energy reduced fuels. This is the approach of *artificial photosynthesis*. Using sunlight is how biology has solved the energy cycle. In nature the solar energy is captured in chemical bonds and one of the enzymes that do it is photosystem II (PSII).

1.2 The processes in Photosystem II

Photosystem II is a protein complex that is kept in the thylakoid membranes in green plants, algae and cyanobacteria. At heart, it splits water into O_2 and H^+ to release high-energy electrons. The electrons are used in further reactions to eventually produce NADPH. The protons are released into the thylakoid lumen to establish a proton gradient across the membrane which drives the ATP production. NADPH and ATP, the "energy currency" of the cells, are used in the so called dark reactions to reduce CO_2 and produce biomass. This long chain of reactions will not start without absorption of photons.

$$2\,H_2O \xrightarrow{4h\nu} O_2 + 4\,H^+ + 4\,e^- \qquad (1)$$

Photosynthesis starts with the absorption of light at one of the chlorophyll molecules generating an excited state. The excited state energy is rapidly transferred between the chromophores within the light-harvesting protein complex via energy transfer until it is trapped at a reaction center at P680.[15,16] P680 is the name of four chlorophyll molecules that have similar absorption wavelengths (675–680 nm) and that share the excitation energy.[17] From this point the electron transfer (ET) reaction chain starts, which is schematically shown in Figure 1.

The excited state, P680*, reduces the first electron acceptor, pheophytin (Pheo), accompanied by a second electron transfer to a firmly bound quinone Q_A within 300 ps generating the charge-separated state, $P680^+Q_A^-$. Migration of the electron over 20 Å away[15,16] and further out avoids relaxation back to the ground state and makes this step efficient. The charge-separated state is also quite long-lived and stable for about 100–200 μs.[18] Furthermore, Q_A reduces another quinone, Q_B, located close to the surface of protein D1. After a second photochemical cycle the

Q_B becomes doubly reduced concomitant with double protonation to form Q_BH_2 and is mobilized into the lipid thylakoid membrane to deliver the electrons further to PSI which produces NADPH. The empty pocket is replaced by a new Q_B molecule to continue the cycle.[19-21]

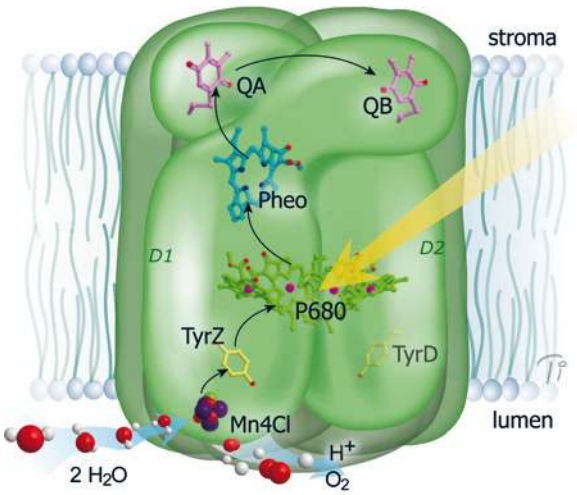

Figure 1. A schematic picture of the redox cofactors within PSII and the reaction pathways for electron transfer. The D1 polypeptide contains the cofactors: Y_Z, Pheo and Q_B and D2 polypeptide contains Q_A and the inactive Y_D. Light energy is captured at the reaction center, P680 which initiates a chain of electron transfers between the subunits, as indicated by the arrows. The catalytic activity of water oxidation occurs at the Mn-cluster.

The recharging of the oxidized $P680^+$ is obtained by electron transfer from a tyrosine, Y_Z, which in turn is reduced by abstraction of an electron from the Mn-cluster: the catalytic center which drives water oxidation. This cycle is repeated four times before two water molecules generate one oxygen molecule. The Mn-cluster, also known as the oxygen-evolving complex (OEC) or water-oxidizing complex (WOC), consist of four Mn atoms and a fifth metal atom, presumably a Ca atom that are linked via μ-oxo bridges. The precise structure of this complex is intensively debated since it is crucial for understanding the mechanism of this catalytic process that is so important for life. The data on crystal structures from X-ray diffraction that are available do not give high enough resolution (3.8–2.7 Å) to reveal the exact structure.[19,22-25] The resolution can be improved by X-ray absorption spectroscopic (XAS) techniques, which in addition yield lower X-ray doses that might otherwise cause damage of the samples. XAS methods has been used to gain additional geometric and dynamic information about the Mn-complex.[26,27] In close connection to this is also the discussion about the mechanism of water oxidation in the Mn-cluster, which is known at a phenomenological level but has to be recognized in detail.

The most widespread mechanistic scheme is the S-state cycle (or Kok-cycle) where the Mn-cluster steps through four oxidation states (S_n, n = 0–4) on its way to catalysis. It starts with the most reduced state, S_0. Each photochemical oxidation of

$P680^+$ is generating the oxidation states ($S_0 \rightarrow S_4$), step by step. During these steps protons are released but the studies on proton release pattern depends on the preparation of the PSII protein.[28] The last step, $S_4 \rightarrow S_0$, occurs spontaneously without light injection. This is a fast step and it has therefore been difficult to study, but it is also the critical step where water is fully oxidized and where O_2 is released from the Mn-cluster. There are, however, different proposals for the characteristics of this intermediate state.[29,30]

1.3 Tyrosine$_Z$ in PSII

Between the light absorbing center, P680, and the OEC is a redox active tyrosine (Y_Z).[31] The main purpose for Y_Z is to carry the electrons from the Mn-cluster, electrons that originates from the water molecules, to fill the hole on $P680^+$. As it is strategically situated right in the middle of the centers of action in PSII, i.e. light absorbing center and OEC, special attention has been paid to the function of Y_Z.[32-36]

There are at least three roles that Y_Z plays as a redox intermediate in PSII: (1) Y_Z acts as a fast electron donor to $P680^+$ and competes effectively with the charge-recombination of $P680^+/QA^-$ and therefore provides a quantum yield close to unity for charge-separation in PSII. (2) The high reducing power of the radical preserves the conditions that are necessary to catalyze water oxidation. (3) Due to the decoupling/coupling of the phenolic proton during electron transfer, charged inter-mediates, which are unfavorable in the non-polar protein environment, are avoided.

The distance between Y_Z and the closest chlorophyll in P680 is about 12–14 Å, while the distance to Mn-cluster is only about 5–7 Å. Due to this proximity to the OEC, the proposed models often suggest that the Y_Z is more or less directly involved in the water oxidation step.[28] Mainly two different models for the mechanistic reaction pattern of Y_Z has evolved. First one: Babcock and co-workers suggested a "H-atom abstraction" mechanismwhere the tyrosyl radical act as the primary H atom abstractor from water bound as ligands in the Mn-cluster in all S-states.[18,34,37] The oxidation of Y_Z is concerted with a release of the phenolic proton to a nearby base and this proton is eventually delivered to the aqueous bulk phase via a network of H-bonded proton acceptors. In the second "proton-rocking" hypothesis the H-bond between Y_Z and the base remains intact but becomes shifted as Y_Z is oxidized/reduced.[38-40] In contrary to the former this model requires charged intermediates since the proton is kept within the protein environment.

Although the ultimate location of the phenolic proton may not be crucial, the detailed mechanism of the first step certainly is. The pK_a of reduced tyrosine in solution is 10 but shifts dramatically to -2 upon oxidation. The electron transfer from tyrosine is therefore coupled deprotonation. The *proton-coupled electron transfer* (PCET) from tyrosine can proceed via three different paths shown in Scheme 1. In the two sequential paths either the proton is transferred prior electron transfer (PTET) or the opposite (ETPT). It is also possible that the mechanism is a concerted

electron proton transfer (CEP). To distinguish between these cases one has to search for the answer in the kinetics of Y_Z oxidation.

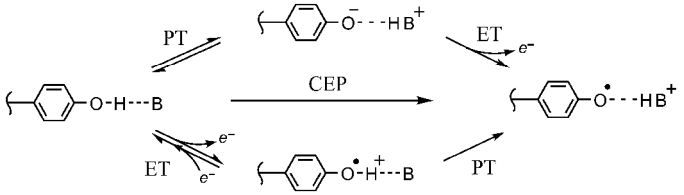

Scheme 1. The possible mechanisms for PCET from Y_Z in PSII with PTET in the upper path, CEP in the middle and ETPT in the lower path.

The kinetics for Y_Z oxidation show a complicated pattern as it is multiphasic and differ between the S-states. From transient absorption changes of the $P680^+$/P680, mainly 3 exponents are extracted from the kinetics. The most dominant is the fastest 20 ns component and is the one that has been attributed to the reduction of $P680^+$ by Y_Z.[36] Due to the small activation energy (≤0.1 eV)[38] and small isotope effect it was concluded that the proton is transferred within a H-bond.[36] The nature of the proton accepting base has been debated but seems to have converged to the common believe that in the intact, active PSII Y_Z is presumably H-bonded to a histidine (His190),[39,41-44] consistent with the crystal structure data.[19]

The mechanism of Y_Z oxidation has been debated. An ETPT mechanism can quickly be eliminated because that path requires a highly charged intermediate which would give high activation parameters. With a redox potential of >1.4 V[34] for the $TyrO^{\bullet}$/ $TyrO^{-}$ couple and ~1.26 V[45] for $P680^+$/P680 couple this gives a uphill reaction of >0.140 eV which cannot explain the observed activation energy of 0.1 eV. Early studies suggested a sequential proton electron transfer with non-limiting proton transfer (PTET).[33] Due to proton tunneling, proton transfer can be vary fast, specially within a H-bond,[a] which establishes a pre-equilibrium situation where the observed rate constant depends on the fraction of tyrosinate which in turn depend on the pK_a difference between Y_Z and the base (ΔpK_a): $k_{obs} = 10^{-\Delta pK_a} \times k_{ET}$. However, it has been speculated what the pK_a of Y and the base actually is and in order to satisfy the above equation the ΔpK_a should be small (<1)[33] which is not consistent with the presumed pK_a of ~7 for the base in Mn-depleted PSII and $pK_a(Y) > 10$.[35,42,46] In more recent studies the CEP mechanism has become the favored one.[46,47] This mechanism avoids charged intermediates which are poorly stabilized in non-polar and fairly rigid medium, like that in the protein. A unified and complete picture of this mechanism it yet to be recognized. PCET reactions are also involved in other steps of the oxygen evolving cycle in PSII.[28,48] In order to understand the processes in PSII it is therefore crucial to develop a good model for PCET reactions. The purpose of this thesis is to give insight of these PCET mechanisms in a model system mimicking the oxidation of Y_Z in PSII.

[a] The rate constant for proton transfer is $k_{PT} = 6\times10^{12}\times10^{-\Delta pK_a}$ s^{-1}, where 6×10^{12} is the collision factor from transition state theory and $\Delta pK_a = pK_a(Y) - pK_a(base)$.

1.4 Artificial photosynthesis

The previous sections perhaps showed how complex and intricate the processes for water oxidation from solar energy in the natural systems really are. This is the demanding picture that a researcher encounters in the pursuit for artificial photosynthesis. An artificial system needs components that: (1) absorb photons and transfer the excitation energy to an reaction site, (2) create a charge-separated state from the excitation energy, (3) transfer the charges to a catalyst and (4) utilize electrons and holes in catalytic reactions. And all these elements need to work together in an efficient way. These are usually schematically represented by a **D-P-A** triad, where **P** is the photosensitizer that absorbs photons. From **P** electrons are ejected to the acceptor **A**, while **D** is the donor, providing **P** with electrons. Uptake of one light quantum gives the charge separated state, $\mathbf{D^{+}\text{-}P\text{-}A^{-}}$. This should be sufficiently long-lived and have sufficient energy to drive the catalytic reactions, i.e. water oxidation at the donor side and reduction of hydrogen into H_2 at the acceptor side. There are numerous synthetic systems that demonstrate one or a few of these properties.[49-56] Major efforts are still needed to construct a fully functional system that can be used for commercial solar fuel production, but understanding and control of charge transport kinetics will be crucial to these efforts.

This thesis work is, in this context, focused on the transport of charges. One of the challenges in artificial photosynthesis is the multi-electron transfer processes needed for water oxidation. Accumulation of electrons increases the stepwise redox potentials and generates high-energy barriers for the subsequent electron transfers. Nature solves this problem by charge compensation. Deprotonation of the redox cofactors avoids high-energy intermediates. Proton-coupled electron transfer processes are therefore important in the construct of an artificial photosystem.

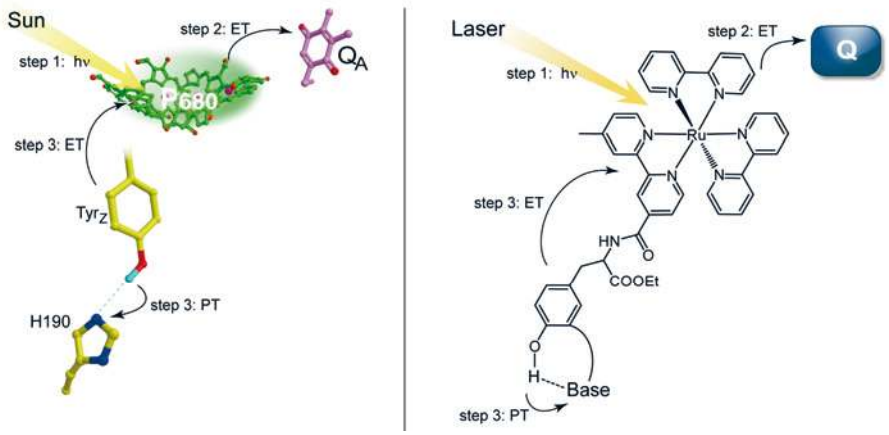

Figure 2. The reaction steps in PSII (left) and in the model system (right). 1) In the first step light energy is captured by excitation of the chromophore. 2) The excited state energy is used in the electron transfer to a quencher. 3) The chromophore is reduced by electron transfer from a tyrosine in concert with proton release to an H-bonding base.

PCET reactions are in this thesis studied in model molecules designed for exactly this purpose. They contain a tyrosine of which the phenolic proton is H-bonded to either an internal or external base (Figure 2). The role of the H-bond and the importance of the base properties are demonstrated in these model complexes. The reaction is initiated by a laser flash at the photosensitizer, a Ru-metal complex (step 1). This generates a metal-to-ligand charge transfer (MLCT) state which is further oxidized by an external quencher (Q) in the solution (step 2). The following step involves the electron transfer coupled to proton transfer from the tyrosine (step 3). The blueprints for these model complexes are obviously inspired from the Y_Z oxidation in PSII.

In the first part of this thesis focus on the effect from internal H-bonds. How does the strength, length and flexibility of the H-bond influence on the kinetics of the PCET reaction? What are the important parameters? These questions are addressed. In the second part we investigate the effects on PCET when either water or the buffer base plays the part as the proton acceptor. Water is a fascinating solvent because of its H-bonding properties. The microscopic picture of the structure of fluid water and the dynamics of it, have for a long time caught many researchers attention and is also crucial for PCET reactions, especially when proton is released to the water. The PCET mechanistic pattern, in this solvent, is intricate and manifold as we show in the model complexes. Moreover, due to the self-dissociation of water, this solvent always provide hydroxide ions (OH^-) and hydronium (H_3O^+) ions as potential proton acceptors or donors, respectively. Another potential proton acceptor is the base form of the buffer. These may vary in their H-bonding properties and basic strength and thereby affect the PCET reactions. Not only is the proton acceptor varied in this study but also the properties of the electron acceptor is tuned. Playing with these parameters opens up for the competition between the PCET mechanisms in a way that makes it interesting to study. I hope that the results in this thesis contribute to the development of good models for this very important and elementary reaction.

2 Theory

The theoretical descriptions of proton-coupled electron transfer, electron transfer and proton transfer have many similarities. This chapter will deal with them one by one. Starting with electron transfer theory[57-62] which was the first one to develop and from which the other two emerged. The general concepts of proton transfer will be presented. The last section concludes this chapter with some theoretical basics for proton-coupled electron transfer theory.

2.1 Electron transfer

The electron transfer (ET) between two molecules in solution can be divided into three steps: (1) the reactants diffuse together to form a *precursor complex*. In this complex all the nuclei in the reactant and surrounding molecules are in their equilibrium position prior electron transfer, (2) the precursor complex reorganizes to a transition state where the electron transfer after vibrational relaxation yields a reorganized *successor complex,* (3) dissociation of the successor complex then yields the products. If the electron transfer is fast compared to the first diffusion step, then the observed rate constant will give no information about the electron transfer step. On the other hand, if electron transfer is slow, then the ET rate constant can be extracted from the kinetics. One way to avoid the consequences from diffusion is to study electron transfer in reactants that are covalently linked. In this way the reactants are considered as being in the precursor complex at all times before they react and (2) is the only step.

The free energy of the reactants depends on all the vibrational movements both within the reactants and the surrounding molecules and defines a many-dimensional potential energy surface. A one-dimensional picture is given in the left hand scheme of Figure 3, where all the nuclear movements are merged into one reaction coordinate. In order for the reaction to occur the reactants has to distort from the equilibrium to a position where the free energy surfaces of the reactants and products cross. At this point electron transfer is possible. Electrons are a much lighter particles than atoms, thus the Franck-Condon principle is employed presuming that the electron is transferred while the nuclear positions remains unchanged. The right hand scheme in Figure 3 illustrates the energy of the electron motion, with the electron positioned on either the donor or acceptor. The horizontal lines represent the total free energy which changes as the systems move along the reaction coordinate. At the equilibrium of the reactants the energy for the reactants is

lower than for the products and the electron remains on the donor atom. At the crossing point the electron is tunneling from the donor to the acceptor while the total energy of the system is conserved. The system then relaxes to give a lower total free energy for the product state and the electron resides on the acceptor.

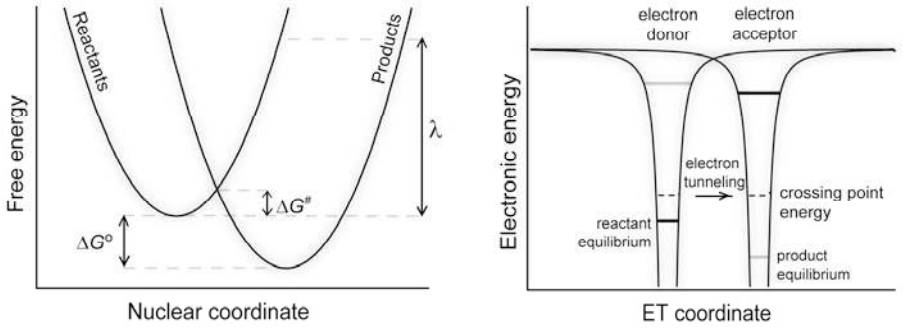

Figure 3. *Left:* One-dimensional potential energy surface of the reactants and products with the activation free energy, $\Delta G^{\#}$, standard free force $\Delta G°$ and reorganization energy, λ, indicated. *Right*: The coulombic energy for the electron in the reactant and product state. The horizontal solid lines represent the overall free energy at the reactants (black) and products (gray) equilibrium position. The dashed lines symbolize the crossing point overall free energy.

Electron transfer kinetics depends on a number of factors that must be considered when calculating the rate constant. In the classical expression by R.A. Marcus,[57] the electron transfer rate constant is expressed by the probability for electron tunneling at the intersection, i.e. the transmission coefficient (κ_{el}), the frequency for passage through transition state (ν_n) and the activation free energy ($\Delta G^{\#}$):

$$k_{ET} = \kappa_{el}\, \nu_n \exp(-\Delta G^{\#}/k_B T) \qquad (2)$$

$$\Delta G^{\#} = \frac{(\Delta G° + \lambda)^2}{4\lambda} \qquad (3)$$

Equation 2 has a general form of an Arrhenius equation with the activation energy expressed by eq. 3. This depends on two parameters: the standard free energy ($\Delta G°$) and the reorganization energy (λ), indicated in Figure 3 (left). The latter is defined as the free energy change upon moving from equilibrium of the reactant state to the coordinate for the equilibrium of the product state without transferring the electron. Thus, it measures the vibrational and configurational changes of the nuclei upon reaction and will give a high activation energy if these are large (assuming $\Delta G°$ is constant and $-\Delta G° < \lambda$). The reorganization is usually divided in an outer-sphere (λ_o) and an inner-sphere (λ_i) contribution. The inner term depends only on the internal vibrational modes, such as bond length changes, and on force constants. When these are treated as harmonic vibrations λ_i is expressed by eq. 5, where r_R^0 and r_P^0 is the equilibrium bond lengths of the reactant and product state, respectively, and f is the reduced force constant.

$$\lambda = \lambda_i + \lambda_o \qquad (4)$$

$$\lambda_i = \frac{1}{2}\sum_i f_i (r_R^0 - r_P^0)^2 \quad (5)$$

$$\lambda_o = \frac{e^2}{4\pi\varepsilon_0}\left(\frac{1}{2a_D} + \frac{1}{2a_A} - \frac{1}{r_{AD}}\right)\left(\frac{1}{\varepsilon_{op}} - \frac{1}{\varepsilon_s}\right) \quad (6)$$

The outer term, also called the *solvent reorganization energy*, λ_o depends on the solvent dielectric properties and distance separating the donor and acceptor. When the solvent is treated as a dielectric continuum and the reactants as spherical molecules this is expressed as eq. 6. Small radii of the donor and acceptor (a_D and a_A, resp.) and a large separation distance (r_{AD}) will give a large λ_o. The terms in the last parenthesis arise because the electrons interact with different parts of the dielectric polarization. ε_{op} (optical dielectric constant) is due to electronic polarizability while ε_s (static dielectric constant) also contains movement of contributions from nuclear polarization (permanent dipol). More polar solvents typically give larger λ_o. e is the charge transferred in the reaction, usually one, and ε_0 is the permittivity in vacuum.

The driving force, $\Delta G°$, for the reaction is given by the vertical displacement of the equilibrium position for the reactant and product (Figure 3). This is usually obtained from electrochemical data, which relates to the free energy change via the Faraday constant.

$$\Delta G° = -nF(E_A° - E_D°) - w_R + w_P \quad (7)$$

$E_A°$ and $E_D°$ are the redox potential for the acceptor and donor, respectively and n is the number of charges transferred. When charged species are brought into close contact the coulombic interaction might be significant and has to be taken into account. The work needed to bring the reactants and products together is given by w_R and w_P, respectively and will be additional terms in eq. 7. Equations 2 and 3 predict a parabolic dependence of log k on $\Delta G°$ (Figure 3, left). For small driving forces, $-\Delta G° < \lambda$, the reaction is in the so called *normal* region where the ET rate constant increases with driving force, illustrated in Figure 4 (left). When $-\Delta G°$ equals λ the numerator in eq. 3 vanishes and the reaction is activation-less and reaches its highest possible rate. Upon further increase of the driving force the reaction becomes activated again, which results in a decrease of the rate constant. This is called the *inverted* region and was predicted by R.A. Marcus in the 50´s but it was not until over 30 years later it was verified experimentally.[63] The reactions studied in this thesis all occur in the normal region with large λ and small $|\Delta G°|$.

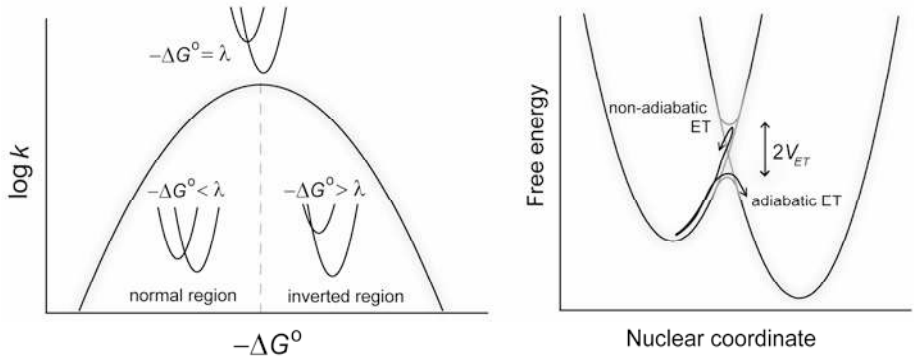

Figure 4. *Left:* Marcus parabola with the normal and inverted region indicated. *Right*: Free energy potentials for the adiabatic and non-adiabatic reaction.

The classical Marcus equation, presented so far, applies only for reactions with $\kappa_{el} \approx 1$, i.e. *adiabatic* electron transfer. Also, in the classical limit, the possibility of nuclear tunneling is not considered. Nuclear tunneling will be important in the inverted region, at very low temperatures where thermal fluctuations are not able to bring the system to the crossing point and for *nonadiabatic* reactions, where $\kappa_{el} << 1$. Quantum mechanical treatment has lead to a semi-classical expression which accounts for nonadiabatic reactions in the high temperature limit:

$$k_{ET} = \frac{2\pi}{\hbar} V_{ET}^2 \frac{1}{\sqrt{4\pi\lambda k_B T}} e^{-\frac{(\Delta G^\circ + \lambda)^2}{4\lambda k_B T}} \qquad (8)$$

V_{ET} is the electronic coupling term which depends on the overlap of the donor and acceptor orbital. Consequently the coupling is largely dependent on the distance separating the electron donor and acceptor, decreasing exponentially with increasing distance. In energetic terms, $2V_{ET}$ is defined as the resonance energy associated with the reactant and product state at the crossing point, indicated in Figure 4 (right). In the non-adiabatic limit, this coupling is smaller than the thermal energy, $V_{ET} < k_B T$ (0.025 eV at 298K). In this case the system mostly remains on the reactant surface when it passes through the intersection region. Only occasionally will it continue to the product surface. For adiabatic reactions, instead, the coupling is large and the surfaces are separated in the intersection region, as illustrated in Figure 4 (right). For these reactions the system will remain on the lower surface as it proceeds through the transition state. However, all the reactions studied in this thesis have small electronic couplings and large donor acceptor distances and are considered as non-adiabatic. Thus, the semi-classical expression in eq. 8 applies.

2.2 Proton transfer

Proton transfer (PT) in solution can be viewed as a simple acid-base reaction: $AH\cdots B \rightarrow A^{-}\cdots HB^{+}$,[b] where B is either a proton accepting solute or a solvent molecule itself. The ability of AH to release the proton to the solution is defined by its pK_a, where K_a is determined by the $AH \leftrightarrow A^{-} + H^{+}$ equilibrium. In water solution the proton never exists as an isolated particle, neither as the H_3O^{+} as commonly thought. Due to the hydrogen bonding nature of water it is presumably shared between several water molecules as, for example, in the *Eigen cation* ($H_9O_4^{+}$) or *Zundel cation* ($H_5O_2^{+}$) or something in between those two.[64] These structural questions are related to the mechanism of proton diffusion in water. This is about three times higher than for H_2O or five times that for ions of similar size as H_3O^{+}.[65,66] This high mobility of H^{+} is usually explained by a *Grotthuss mechanism*, which involves a shuttling of protons between successive water molecules rather than a diffusion of the entire Eigen or Zundel cation. Also, the diffusion controlled collision between H^{+} and an uncharged species is faster (4×10^{10} M^{-1} s^{-1})[67] than a diffusion limited reaction between other species.

A more general case is the proton transfer between two different acid-base pairs in the presence of water as solvent. In this case the equilibrium constant is defined by the difference in pK_a of AH and HB^{+}, i.e. $\Delta pK_a = pK_a(HB^{+}) - pK_a(AH)$. Provided that the proton donor is more acidic than the acceptor ($\Delta pK_a > 0$) the forward step will be activation-less and only be limited by diffusion, giving a rate constant of ca. 1×10^{10} M^{-1} s^{-1}. Systems that behave in this way have been termed *normal* acids by Eigen, and are mainly valid for proton transfer between electro-negative atoms such as oxygen and nitrogen.[68,69] Consequently, the backward reaction step, $AH\cdots B \leftarrow A^{-}\cdots HB^{+}$, will have a rate constant that depends on the pK_a difference: $10^{10-\Delta pK_a}$ M^{-1} s^{-1}.

The early theoretical description for proton transfer was based on a transition state (T.S) model where the energy diagram has two minima representing the reactant and product. The activation barrier separating the reactant and product well is a result of the necessity to stretch the A–H bond in order to reach the product. To account for differences in proton transfer rate constant for hydrogen (H) and deuterium (D), i.e. kinetic isotope effects (KIEs), this classical picture was refined by including zero point energies for H and D. Due to deuterium's larger mass it will have a smaller zero point energy than hydrogen leading to a higher activation energy for deuterium. Thus, in this semi-classical view k_H/k_D will approximately equal $\exp(\Delta E_a/RT)$, with ΔE_a given by the difference in activation energy for H and D. While this could be estimated from the experimental determined stretching vibrations of O–H/O–D bonds it was expected that k_H/k_D should have a value of 10.6. This was a maximum value since the T.S. might also have a zero point energy that would decrease ΔE_a. However, larger KIEs than that have been observed

[b] Note that AH and B might also be charged species.

experimentally and the T.S. model was further modified by the so called *tunneling correction.*[70] This accounted for the quantum mechanical nature of the proton for which the uncertainty of the proton location is given by the de Broglie wavelength. If this exceed the energy barrier width the proton can cross to the product state below the T.S. energy, via tunneling. This effect, however, was only supposed to be important close to the barrier top where the width is narrow and the A–H bond stretch still has to be thermally activated to some extent.

The theoretical picture, currently most used, is quite different from the historical described above. It is broadly accepted that the proton should be treated quantum mechanically due to its small mass. As with electrons, proton movements can be separated from the movement of the other nuclei due to the large difference in mass. Thus the proton may also be transferred in a tunneling event while the other atoms remain frozen. Figure 5 (left) shows the energy profiles for the reactant and product state where the reaction progress is given by a solvent coordinate.[71-74] Note the similarity with the Marcus electron transfer theory. The right hand profiles in Figure 5 depict the proton free energy curves at three different solvent configurations: A, B and C. The two minima *d* and *a* represent the proton residing on the donor and acceptor, respectively. Note that the shape of the proton profiles changes with the solvent coordinate, particularly the relative energy of the *d* and *a* well. At the reactants equilibrium coordinate (A) the proton energy profile is asymmetric favoring proton to stay bound to the acid. At the crossing point *d* and *a* are degenerate and proton tunneling from *d* to *a* is possible. While the system relaxes from B to C the proton profile shape changes, lowering the *a* well energy in favor for the proton residing on the acceptor.

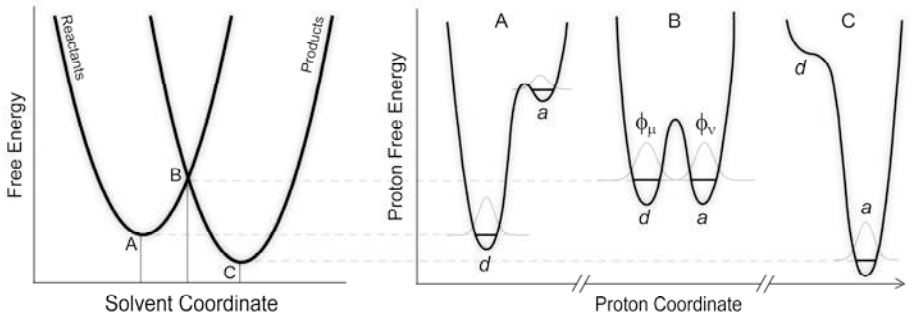

Figure 5. *Left:* Free energy surfaces for the reactant and product along with the reaction coordinate *Right*: Proton free energy profiles for the solvent coordinates at reactant state (A), transition state (B) and product state (C). The two minima in each potential curve represent the donor (*d*) and acceptor (*a*) state and the horizontal lines are the diabatic energy levels.

We may consider two cases for proton transfer, the first is *adiabatic* PT where the surroundings have rearranged to establish a symmetric proton potential, for which the lowest proton vibrational state is above the barrier. Although the proton motion is not tunneling in this case, it is still quantum[72] and the vibrational wave function at the transition state is delocalized over both the minima (left in Figure 6). The other case is the *nonadiabatic* PT where the lowest proton vibrational energy state is

below the barrier in the symmetric proton potential. In this case the proton is tunneling through the barrier to reach the product state. The rate expression for proton transfer deviates between the models but has a general form very similar to that for non-adiabatic electron transfer in eq. 8.

The probability for proton tunneling depends on proton vibrational wave function overlap between the reactant and product state, and is given by the dirac notation, $<\phi_\mu|\phi_\nu>$, where ϕ_μ and ϕ_ν are the reactant and product wave function, respectively. As shown in Figure 6 wave function overlap is strongly dependent on the distance separating the donor and acceptor, $d_{A\cdots B}$, and thus the H-bond length in the AH$\cdots$B couple. For long H-bonds this overlap is small giving a small probability for proton tunneling and therefore smaller PT rates. As the distance is decreased the barrier shape changes and the wave function overlap increases. This means that heavy nuclei configurations with compressed donor-acceptor distance will enhance the overlap and consequently increase the proton tunneling rate. The left hand profile shows an example of a short H-bond. In this case the large overlap leads to a proton totally delocalized between the donor and acceptor atom. In this case the proton is not tunneling through the barrier but is rather distributed over a larger range in the H-bond, in a so called *low barrier hydrogen bond* (LBHB). The PT studied in chapter 5 occurs with $d_{A\cdots B}$ of ca. 2.5 Å which can be considered as intermediate H-bonds.[75] These are consistent with tunneling of the proton in a nonadiabatic reaction.

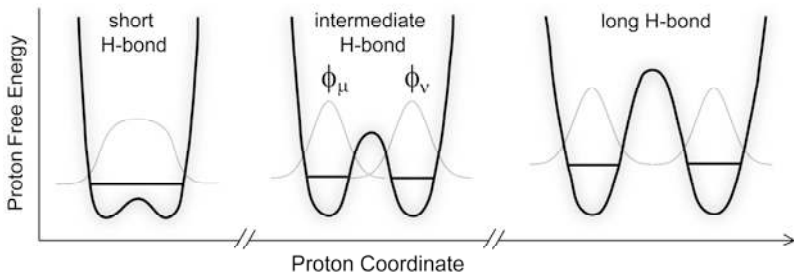

Figure 6. The effect on electronic coupling and proton vibrational overlap on H-bond distance.

Significant kinetic isotope effects are usually used as an evidence for the proton being involved in the rate determining step. For adiabatic PT the only parameter that depends on the isotope is the zero point energy. Thus, the kinetic isotope effect arises from difference the activation energy for H and D. As we saw above, this can only give rise to small KIEs. In contrast, due to the extreme KIEs sometimes observed experimentally a description that allows for tunneling of the proton is required.[76,77] For nonadiabatic PT the KIE is explained by the wave function overlap difference between H and D. The deuterium vibrational wave function is more localized than that of the hydrogen. Consequently, for similar tunneling distances, the overlap will be smaller for the heavier isotope giving a reduced tunneling probability. This difference is particularly important at large tunneling distances, but becomes less pronounced at small donor-acceptor separation. Therefore one would expect an increase in KIE with H-bond length.

Another parameter to consider is the excitation of vibrational states. These have more extended wave functions and therefore larger overlap of the reactant and product state. For the heavy isotope, with smaller energy difference between the excited states and thus a higher Boltzmann population, the excited states give a larger contribution to the transfer rate in D than in H. This results in smaller KIEs when the path through excited states becomes significant.

Proton tunneling requires a close contact of the donor acceptor to occur. Proton tunneling distances are usually about 0.5 Å or less. This is in contrast to electron tunneling which can extend over several ångströms. For such large distances the electron donor-acceptor interaction is small and ET can usually be treated as nonadiabatic. While this treatment often is valid also for PT the adiabatic regime might be entered due to the close contact in PT. Further, higher states are more easily populated in the proton energy profile due to the smaller energy difference between ground and excited states. This is important for interpreting KIEs, as discussed above.

2.3 Proton-coupled electron transfer

So far in this chapter electron transfer and proton transfer has been treated separately. But due to the electronic changes the transfer of these charged particles involves, they are often coupled in a way the that movement of one will induce a shift in the position of the other. Such processes are termed *proton-coupled electron transfer* (PCET) and have in the recent years been reviewed extensively.[78-89] PCET reactions are usually categorized by the relative directionality of H^+ and e^- transfer. The terminology may differ between authors, but in this thesis *unidirectional* PCET defines the reaction when H^+ and e^- share the same donor and acceptor, while in a *bidirectional* PCET they are transferred in opposite direction to (or from) separate acceptor (or donor) molecules. Another subgroup of PCET is hydrogen atom transfer (HAT) reactions in which H^+ and e^- moves together in the same path as a hydrogen atom. HAT and non-HAT reactions are separated in terms of adibaticity of PCET[90] but also by the orbitals involved.[91] In HAT reactions H^+ and e^- share the same molecular orbitals in the donor and acceptor, while in non-HAT they do not.[48] However, the reactions studied in this thesis are all bidirectional PCET.

PCET reactions are usually not difficult to identify as the reactants and products can be observed experimentally. Instead, the debate in the PCET community often concerns which mechanistic route is leading to products. Three different mechanisms are usually considered for PCET reactions. These are the stepwise with either electron or proton transferring first, or concerted step where H^+ and e^- transfers simultaneously. The nomenclature of these steps deviate amongst authors, but in this thesis the term ETPT will be used for electron-first mechanism, PTET for proton-first mechanism and CEP for the concerted transfer of the electron and proton, as indicated in Figure 7a.

The theoretical treatment for PCET reactions has developed from the Marcus picture for ET and PT where the free energy of the system is given by the solvent coordinate.[81,86] For PCET this results in a three-dimensional picture with four paraboloids representing the diabatic states of reactants, products and intermediates of the stepwise paths. The coordinates are given by movements of the heavy atoms in the reactants and solvent rearrangements in the direction for electron or proton transfer, respectively. It will not be reviewed in detail here how this is treated mathematically, but more on a conceptual level. Since ET and PT are both treated as quantum processes it might be difficult on a theoretical level to define a concerted movement of those.[90] However, in this thesis a CEP is defined as a process going through one common transition state, illustrated in Figure 7b. Experimentally, this means that no intermediate can be observed. The CEP reaction coordinate is thus given by a diagonal cut through the reactant and product minima. In analogy with the two-dimensional free energy diagram the reaction free energy, ΔG°_{CEP}, and reorganization energy, λ_{CEP}, are given by the reactant and product paraboloid in this coordinate.

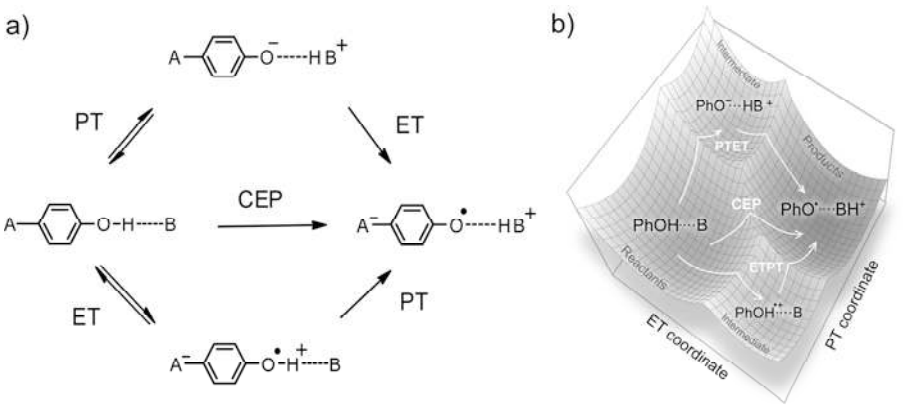

Figure 7. a) Possible mechanisms for PCET in phenol oxidation: PTET (top), ETPT (bottom) and CEP (middle). b) Schematic picture of the free energy landscape with the states representing the reactants, products and intermediates of PCET. Note that crest depicts the crossing points of each paraboloid. The individual steps may still be nonadiabatic.

The driving force for CEP is determined by the E° and pK_a of the donor and acceptor, but these properties are also related to each other. Consider for example phenol being a quite weak acid in its reduced state with a pK_a = 10. Oxidation of phenol to the radical cation ($PhOH^{\bullet+}$) drops the pK_a to -2, making it a very strong acid. Similarly, the E° for protonated redox couple $PhOH/PhOH^{\bullet+}$ is ca. 1.5 V vs NHE, while E° for deprotonated redox couple $PhO^{-}/PhO^{\bullet}$ is ca. 0.7 V. The presence of the proton makes the phenol 0.8 V harder to oxidize than when the proton is absent. These effects are not unusual and similar shift can be seen in other compounds. A shift of 59 mV in E° is balanced by one unit change in pK_a by Nernst equation. Thus, the driving force for CEP consists of two additive contributions: one from ET and one from PT (eq. 9 – 11). Note that this is just the thermodynamics of

corner steps in the square-scheme, where the driving force is related to E° by Faraday constant and E°_{donor} in this case is the redox potential for the $PhO^-/PhO^\bullet$.

$$\Delta G^\circ_{CEP} = \Delta G^\circ_{ET} + \Delta G^\circ_{PT} \quad (9)$$

$$\Delta G^\circ_{ET} = -nF(E^\circ_{acceptor} - E^\circ_{donor}) \quad (10)$$

$$\Delta G^\circ_{PT} = -RT \ln 10 \times \Delta pK_a \quad (11)$$

Driving forces are insufficient to predict the kinetics of PCET reactions. The other parameters that might be important as well are the reorganization energy and coupling constant. Comparing ET-limited ETPT and unidirectional CEP, the latter should give smaller λ_o because these is no formal charge transfer. But same might not be true for a bidirectional CEP. λ_o should be affected by the additional release of the proton. It has be suggested that this effect is just additive giving $\lambda_o = \lambda_o(ET) + \lambda_o(PT)$.[92] The coupling constant will depend on the adiabaticity of the PCET reaction. For nonadiabatic reactions it can be approximated as the product of the electronic coupling and the proton vibrational overlap: $V_{\mu\nu} \approx V_{ET} \langle \phi_\mu | \phi_\nu \rangle$.

In order to determine the characteristics of CEP and conditions favoring the separate paths, PCET is in this thesis studied in a model system for which the donor is a phenol, covalently linked to a ruthenium complex as electron acceptor. The proton acceptor is varied between being an *intra*-molecular H-bonding base, an *inter*-molecular H-bonding base or molecules in the water solvent itself. Note that this and previous work in this lab are the first examples in literature where the PCET is studied in a covalently linked system in aqueous solution. This allows for direct determination of the PCET rate constant without complication from diffusion. In addition, since water is used as the solvent, effects from pH or H-bonding to H_2O can be studied, and makes it a convenient model system for the PCET processes that are occurring in biology.

3 Experimental part

This chapter gives a general description of the main experimental techniques used in this thesis. The important reactions preceding and following the PCET are presented together with some characteristics of the reactive species.

3.1 Transient absorption spectroscopy

In transient absorption spectroscopy the change in absorbance of a sample is measured as a function of time after excitation by a light pulse. It is used to measure lifetimes of excited states or other species for which the extinction coefficient is dissimilar for the reactants and products. Absorption changes and emission lifetimes with dynamics as fast as ca. 10 ns can be probed with the laser flash-photolysis setup schematically illustrated in Figure 8. In this, the excitation light is generated by a Q-switched Nd:YAG laser and that, after passing through an OPO, produces ca. 7 ns laser pulses at 460 nm. The analyzing white light (generated by a 150 W Xe-lamp) is directed through the sample, perpendicular to the excitation light path. After the analyzing light is transmitted through the sample it enters a monochromator before hitting the photo multiplier (PMT). The analogue current signal is digitalized by an oscilloscope and transferred further to a computer as readable data. Examples of traces are shown in Figure 9.

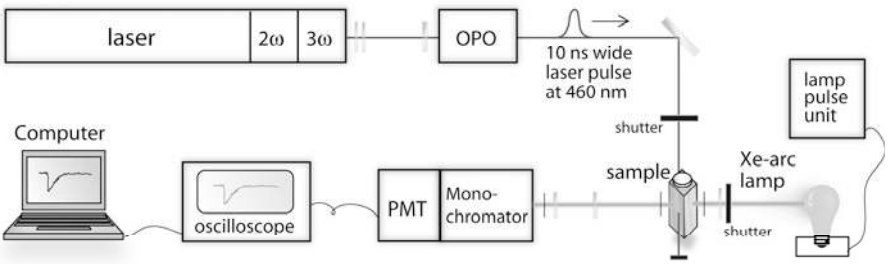

Figure 8. Schematic presentation of the laser flash photolysis setup.

3.2 Chemical components and reactions

All experiments were done with H_2O as the solvent. Water strongly interact with the reactive species due to its high polarity and H-bonding properties. This may make the analysis more intricate than for a more “passive” solvent, but also more

interesting as it is closer to the conditions in nature. Isotope effects are measured in deuterated solvent (D_2O), assuming that the H/D exchange of the phenolic proton is faster than the sample preparation. pD is determined by withdrawing 0.4 pH units from reading of a standard pH meter, to correct for weaker electrode response to D^+ than H^+.[93]

3.2.1 Excitation and quenching reaction

In this thesis the oxidized state of the metal complex, $[Ru(bpy)_3]^{3+}$, and derivatives of this is used as an oxidative reagent. This is generated by oxidative quenching of the excited state: $*[Ru(bpy)_3]^{2+}$ (short: $*Ru^{II}$). $[Ru(bpy)_3]^{2+}$ (Figure 9a) absorbs strongly in both the UV and visible region with a broad band peaking at ca. 450 nm.[94] Excitation of $[Ru(bpy)_3]^{2+}$ into this band populates the singlet ^{1}MLCT-state (metal-to-ligand-charge-transfer state) that is rapidly (<1 ps) converted lowest excited ^{3}MLCT-state with near unity quantum yield efficiency.[95,96] In this thesis an excitation wavelength of 460 nm is used to generate $*Ru^{II}$ (eq. 12). The transient absorption spectrum of $*Ru^{II}$ relative to the Ru^{II} ($\Delta Abs = Abs(*Ru^{II}) - Abs(Ru^{II})$) is partly a broad negative spectrum with a minimum around 450 nm. The ^{3}MLCT-state is long-lived ($t \approx 0.6$ µs in water) and decays to the ground state, giving phosphorescence with 0.04 quantum efficiency.[97] This gives a broad orange-yellow emission around 600 nm. Probing the transient absorption at 450 nm or emission at 600 nm of $*Ru^{II}$ gives the traces illustrated by the dashed blue and black lines, respectively, in Figure 9b.

Thanks to the long-lived excited state of Ru^{II} the bimolecular reaction with an external quencher is very probable. Here, the aim is to generate the oxidized state Ru^{III} by an external electron acceptor fast enough in order to have a well-defined time zero for the following PCET reaction. Additional requirements are that the electron acceptor should not interfere with the subsequent PCET reaction or give spectroscopic features that overlap those of the PCET reactants. The bimolecular reaction between $*[Ru(bpy)_3]^{2+}$ and methyl viologen (MV) (Figure 9b) occurs with $k_q = 5.6\times10^9\ M^{-1}\ s^{-1}$ and a quantum yield of ca. 0.4.[98] This reaction gives the reduced methyl viologen radical ($MV^{\bullet+}$) and the oxidized Ru^{III}, as given by eq. 13.

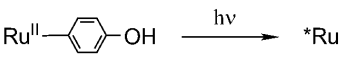

(12)

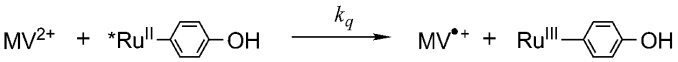

(13)

The oxidized methyl viologen (MV^{2+}) is a colorless species while $MV^{\bullet+}$ gives a broad absorption at 600 nm and a sharp more intense one at 400 nm.[99] Figure 9b shows an example of traces from samples with 0 and 20 mM MV and ca. 30 µM Ru^{II} complex. Note that the life time of $*Ru^{II}$ is shortened in the sample with 20 mM MV, as seen in the 600 nm emission signal and the 450 nm ΔAbs signal which are signatures of $*Ru^{II}$. The generation of $MV^{\bullet+}$ is seen in the rise of the ΔAbs at 600 nm (red trace). Since the concentrations of the Ru complex is much smaller than

the quencher concentration ([Ru] ≈ 30 µM and [MV^{2+}] = 6 to 160 mM) the quenching rate is pseudo-first order in [MV^{2+}]. Figure 9c shows the traces for two different MV^{2+} concentrations. For 160 mM MV^{2+} the quenching occurs within 10 ns. These conditions are used for samples with high PCET rates, at e.g. high pHs for **RuY** (see chapter 5).

3.2.2 The PCET and recombination reaction

The difference absorption spectrum of $[Ru(bpy)_3]^{3+}/[Ru(bpy)_3]^{2+}$ has a broad negative absorption around 450 nm. This is shown by the blue spectra in Figure 9h where the transient spectra are measured for two Ru complexes at 400 ns after the excitation pulse when the quenching reaction has reached to completion. The amount of Ru^{III} produced is also seen by the 450 nm signal which is non-zero at long times in Figure 9b and c. Figure 9d shows the same trace but extended to longer time scales. Here the quenching reaction is only seen as a sharp peak at time zero and the initial amplitude after the sharp peak at 450 nm gives the amount of Ru^{III} generated directly after the quenching.

The reduction of Ru^{III} by phenol can be followed by the 450 nm decay back to zero (eq. 14 and Figure 9d). At this wavelength the absorption of $MV^{\bullet+}$ is very weak. Figure 9e shows the kinetic traces for PCET within a Ru-PhOH complex at pH 9 and pH 7 giving two different observed rates. k_{PCET} is here obtained by fitting the 450 nm trace to an exponential decay. The PCET from phenol can also be followed at 410 nm where $PhO^{\bullet}$ has a sharp double peak.[100,101] However, due to the small ΔAbs signals (usually around 0.01 abs units) and the noise levels these experiments provide, it is usually difficult to separate the $PhO^{\bullet}$ signal from the 400 nm signal of $MV^{\bullet+}$. Instead, the traces in Figure 9f and h are measured with $[Ru(NH)_6]^{3+}$ as an external quencher. This reacts with similar k_q as for MV (k_q = 2.4×10^9 M^{-1} s^{-1})[97] and gives no transient absorption signals in the visible region. Thus, is serves as a nice complement that opens up spectral regions that are otherwise masked by $MV^{\bullet+}$. The transient spectra of two Ru-PhOH complexes using $[Ru(NH)_6]^{3+}$ as quencher were measured and are shown in Figure 9h. They show the characteristic peak of $PhO^{\bullet}$ around 410 nm at times where PCET is complete. The recombination reaction between $PhO^{\bullet}$ with $MV^{\bullet+}$ (eq. 15) occurs on the µs to ms time scale and is usually much slower than the PCET rate, seen in Figure 9g.

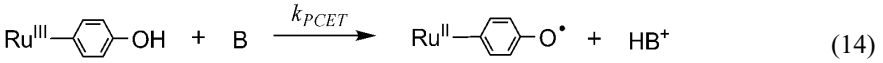

(14)

(15)

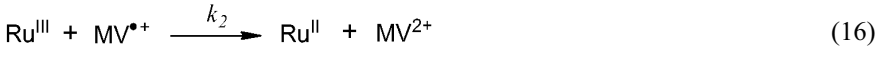

(16)

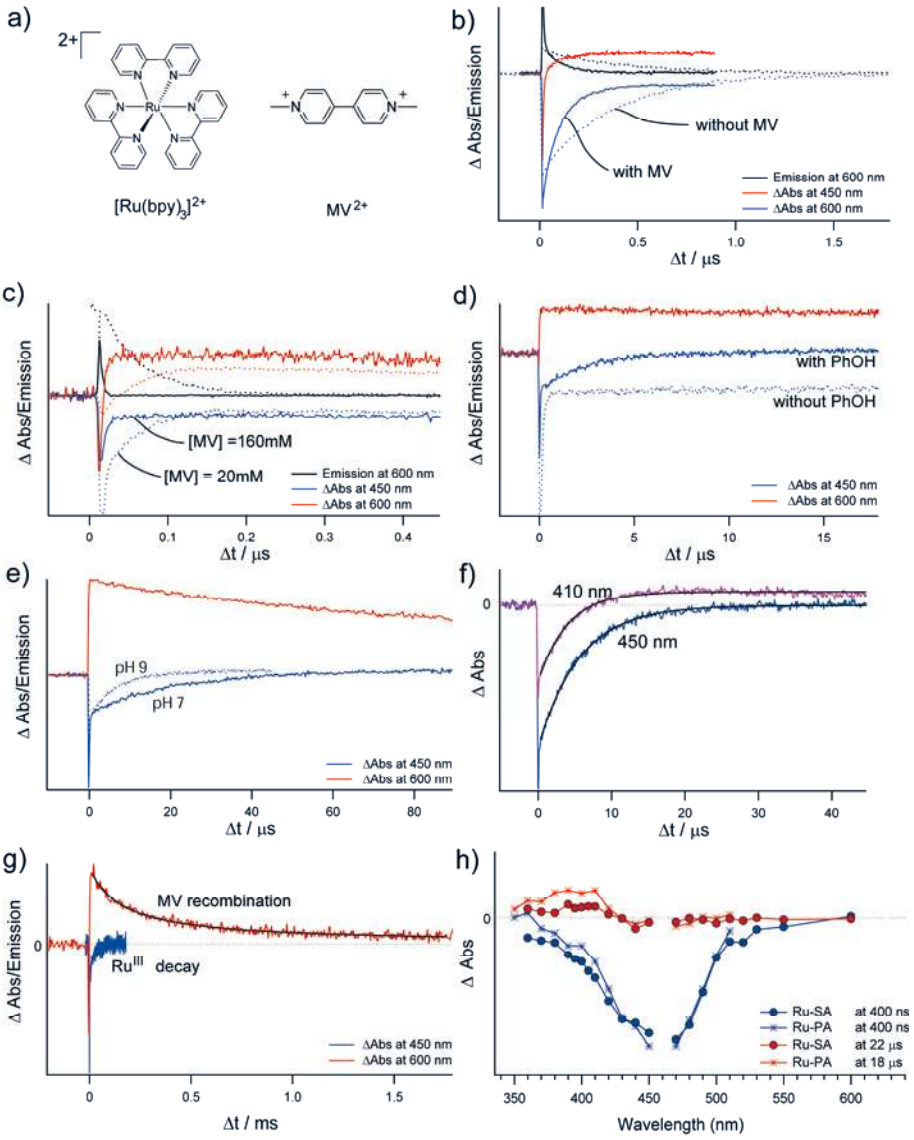

Figure 9. a) Structures of $Ru(bpy)_3^{2+}$ and methyl viologen (MV) in. b)−h) shows examples of transient absorption and emission traces and for samples containing at least a Ru complex dissolved in aqueous solution. b) With 0 and 20 mM MV. c) With 20 and 160 mM MV. d) With ca. 20 mM MV and with and without phenol. e) Kinetic traces of **Ru-Y** at exemplifying the traces two different PCET rates. f) The generation of $PhO^{\bullet}$ at 410 nm and decay of Ru^{III} at 450 nm. g) Comparison of the bimolecular $MV^{\bullet+}$ decay at 600 nm and Ru^{III} decay at 450 nm. h) Transient absorption spectra of **Ru-SA** and **Ru-PA** at two different times: Blue curves represent the Ru^{III} spectra and red curves represent the $PhO^{\bullet}$ spectra.

The reduction of Ru^{III} by PhOH is usually much faster than the recombination reaction between Ru^{III} and $MV^{\bullet+}$ (eq. 16). In a sample where there is no phenol added, these recombine with a second order rate constant $k_2 = 2.4\times10^9\ M^{-1}\ s^{-1}$.[97] About 1 μM of Ru^{III} and $MV^{\bullet+}$ is generated by one laser flash under the conditions

used here. This gives an observed half life $\tau_{½} \approx 1$ ms which is much slower than most of the PCET rate constants. For $k_{obs} < 10^4$ s^{-1} the single exponential recovery of the Ru^{II} complex was corrected for the recombination reaction with $MV^{\bullet+}$ using $[Ru^{II}] = [Ru^{II}]_0 e^{-kt} \cdot [MV^{\bullet+}]_0/(1 + k_{SO} \cdot [MV^{\bullet+}]_0 \cdot t)$, where k is the rate constant for intramolecular reaction with PhOH and k_{SO} is the second order rate constant for the $MV^{\bullet+}$ recombination obtained from the decay of the 600 nm signal.

Note that both the 450 nm signals in Figure 9e decay back to zero before the one at 600 nm. This means that all Ru^{III} is reduced to Ru^{II} by phenol and thus the recombination reaction (eq. 16) does not compete with the PCET. However, for very slow PhOH oxidations (where the correction for $MV^{\bullet+}$ recombination is insufficient) the inference from $MV^{\bullet+}$ may be an issue. Then the choice is to use a sacrificial electron acceptor as $[Co(NH_3)_5Cl]^{2+}$. This oxidizes $*[Ru(bpy)_3]^{2+}$ with $k_q = 9\times10^8$ M^{-1} s^{-1} and decomposes into non-reactive products: Co^{2+}(aq), NH_4^+(aq) and Cl^-(aq).[97] The reactants and products for this have very weak transient absorption in the visible spectrum that could interfere with the Ru and PhOH signals. However, the irreversibility is at the same time a disadvantage. Due to the inability of the electron acceptor to return the electron to $PhO^{\bullet}$ the latter dimerizes and the concentration of active reactants will decrease for every laser shot. This makes the averaging of data, which is necessary to get reliable data, more difficult.

Another competitive reactant is oxygen. O_2 quenches excited state $*[Ru(bpy)_3]^{2+}$ very effectively generating oxygen ion O_2^-.[97] To avoid competitive quenching by O_2 and reduction of Ru^{III} by O_2^-, the samples were de-aerated by purging with argon gas for at least 10 minutes before and during the measurement.

4 PCET from phenols with an internal hydrogen bond

In chapter 1 it was described how the electron transfer from Y_Z in PSII is coupled to deprotonation via a more or less permanent H-bond to His190. This chapter deals with PCET from phenols with intramolecular H-bonding bases, carboxylate groups, which act as the primary proton acceptor. Throughout the chapter, two phenols are compared, in which a carboxylate group is linked either directly to the phenol or via a methylene group and have therefore not the same H-bond properties. This chapter presents the kinetics and the mechanisms of PCET and gives the detailed insight into the parameters obtained from numerical modeling of the experimental data summarizing paper **I**, **III** and **IV**.

4.1 Reaction free energies

The phenols with an intramolecular H-bonded carboxylate group are shown in Scheme 2, where **SA** and **PA** reacted with $[Ru(bpy)_3]^{3+}$ in a bimolecular reaction and ***p*-SA** and ***p*-PA** were used as non-H-bonded reference compounds. But since bimolecular reactions can be diffusion limited, which limits the analysis of the PCET reaction, the study was complemented with synthesized compounds where $[Ru(bpy)_3]^{3+}$ and the H-bonded phenols are covalently linked, **Ru-SA** and **Ru-PA.** These made it possible to measure the PCET rate constant *directly*. But before the kinetics is presented, the energetics for the different mechanisms of PCET from these phenols will be presented.

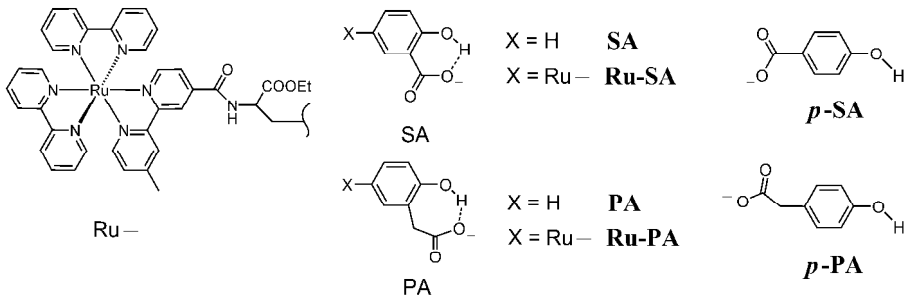

Scheme 2. Structures of the compounds: **SA** and **PA** are the H-bonded phenols compared in this study which reacted bimoleculary with $[Ru(bpy)_3]^{3+}$, or intramoleculary as in **Ru-SA** and **Ru-PA**. ***p*-SA** and ***p*-PA** are the non-H-bonded *para* analogues, used as reference compounds.

The three mechanistic path ways, presented in chapter 2, are sketched in Scheme 3 for PCET from the H-bonded phenols. These are all followed by a fast deprotonation of the carboxylic group to water. As will be discussed below, both the stepwise paths can be excluded, leaving only CEP as the mechanism explaining the kinetic data. Moreover, the thermodynamic analysis below shows that both the stepwise paths require unfavorable uphill initial steps, while the concerted transfer of e^- and H^+ is energetically favored.

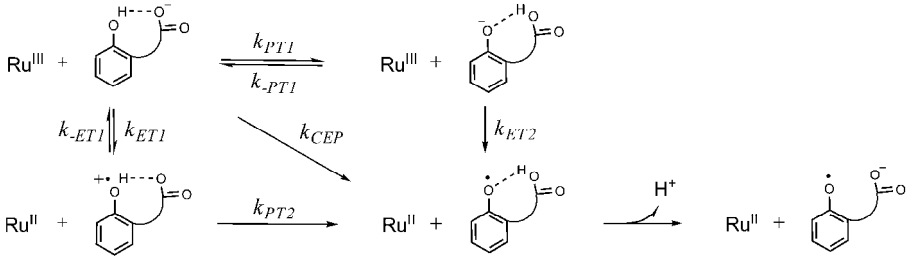

Scheme 3. Mechanistic scheme over the possible paths for PCET from the H-bonded phenols.

4.1.1 Driving force for the stepwise mechanisms

The experimental redox potential of the doubly deprotonated form of **SA**, **PA**, ***p*-SA** and ***p*-PA**, as well as the pK_a for the first and second deprotonation, were determined in paper **I** and are shown in Table 1. For a PTET mechanism, where the first step is a rapid PT equilibrium, the redox potential of the phenol for the second ET step is then given by $E°_{\mathrm{PhO}\bullet/\mathrm{PhO}^-}$. This step is always downhill as the redox potential for all the electron acceptors discussed in this thesis is >1.1 V. The overall rate might be slow anyway because only the fraction that has a deprotonated phenol will continue to the ET step for the H-bonded phenols. This fraction is given by $10^{-\Delta \mathrm{p}K_a}$ (where $\Delta \mathrm{p}K_a = \mathrm{p}K_a(\mathrm{OH}) - \mathrm{p}K_a(\mathrm{COOH})$) and is very small since $\Delta \mathrm{p}K_a > 6.6$.

In the ETPT mechanism ET precedes PT with an uphill step. Here the relevant potential is that for the protonated phenol couple, $E°_{\mathrm{PhOH}\bullet+/\mathrm{PhOH}}$. Due to the low p$K_a$ of $\mathrm{PhOH}^{\bullet+}$ these potentials are difficult to measure. Instead these were calculated from $E°_{\mathrm{PhO}\bullet/\mathrm{PhO}^-}$ with the assumption that the difference in potential for the protonated and deprotonated redox couple is similar for this series of phenols. From these estimated values the $\Delta G°$ for the ET step of ETPT is +0.22 V for **SA** and +0.16 V for **PA**. The sequential PT is fast and downhill as the OH group in the radical cation is much more acidic than the acid form of the proton accepting COO^- group. $\Delta G°$ for PT is ca. -0.6 eV for **SA** and -0.4 eV for **PA**, given by eq. 11 in chapter 2.

Table 1. Redox potentials and pK_a-values of the H-bonded phenols studied. For details, see paper **I** and **IV**.

	SA	***p*-SA**	**PA**	***p*-PA**	phenol
pK_a(OH)	13.5	9.3	10.9	10.3	10.0
pK_a(COOH), experimental	3.1	4.5	4.3	4.3	–
pK_a(COOH)$_{ox}$, calculated	3.5	–	4.5	–	–
$E°_{PhO^•/PhO^-}$ (V)[I]	0.77	0.90	0.71	0.75	0.78
$E°_{PhOH^{•+}/PhOH}$ (V)[II]	1.48	1.61	1.42	1.46	1.49
$\Delta G°_{HB}$, (V)[III]	+0.10		-0.17		

[I] Measured by pulse radiolysis in paper **I**. [II]Calculated from $E°_{PhO^•/PhO^-} + 12\times RT\ln 10/F$. [III] Estimated from DFT calculations and eq. 18, see text.

4.1.2 Driving force for the concerted mechanism

For the CEP mechanism the potential of interest is that for the PhO$^•$···COOH/ PhOH···COO$^-$ couple, $E°_{HB}$ in Figure 10. This is given by the potential for the doubly deprotonated redox couple and the difference in pK_a of the phenol and carboxylate group:

$$E°_{PhOH-COO^-/PhO^•-COOH} =$$

$$E°_{PhO^--COO^-/PhO^•-COO^-} + 0.059\ \text{eV} \times (\text{p}K_a(\text{OH}) - \text{p}K_a(\text{COOH})) \quad (17)$$

$$\Delta G°_{HB} = -nF\times(E°_{Ru^{II/III}} - E°_{PhOH-COO^-/PhO^•-COOH}) \quad (18)$$

Thus, the driving force is determined by the internal base mainly via the pK_a of the conjugate acid. There may also be a contribution from the difference in H-bond energies between the reduced and oxidized form, but this is in general small, less than 0.2 V.[102] It was pointed out by Mayer and co-workers that the effect from hydrogen bonding is often misinterpreted as it is assumed that the lower redox potential observed for the H-bonded phenols is due to the H-bond strength.[102,103] In addition, the H-bond binding energy of the PhOH-base form is generally more stabilizing than in the more electron deficient PhO$^•$-H$^+$base form, and it would in that case rather *increase* the redox potential than lower it. The negative potential shift observed for phenols in the presence of hydrogen bonding bases is therefore not because of the hydrogen bond but because of the presence of a good proton acceptor.

The potential for CEP in eq. 17 can be found from the formal potential ($E°'$) at pH = pK_a(COOH). At this pH the $\Delta G°'$ for proton transfer between the COOH group and bulk water is zero, illustrated by the vertical reactions in Figure 10a. $E°'$ is the pH-dependent potential for the thermodynamic equilibrium between the PhO$^•$/PhOH couple where the proton is released to the bulk as shown by the horizontal reactions in Figure 10a (equation 25, in chapter 5). The potential for **SA** at pH = 3.1 may be determined electrochemically but is complicated partly due to two-electron oxidation.[104,105] Instead, it was estimated from its value of $E°_{PhO^--COO^-/PhO^•-COO^-}$ at basic pH and a Nernstian behavior on pH, illustrated by the solid line in Figure 10b

and given by eq. 17. The driving force for CEP from H-bonded phenols is then given by eq. 18.

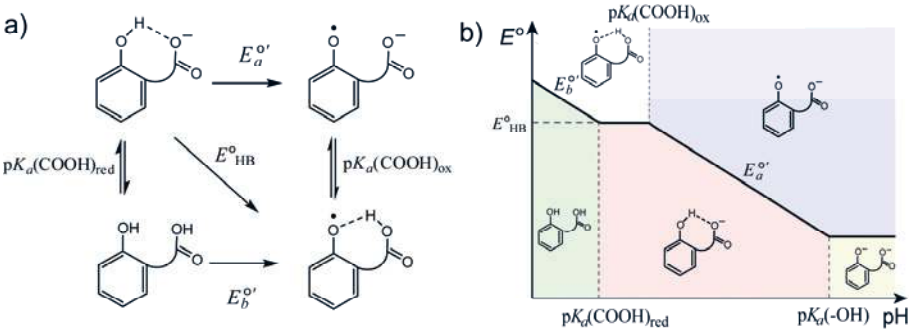

Figure 10. *a)* Scheme for calculating the $E°_{HB}$; redox potential for the CEP mechanism within the H-bonded compounds, **SA** and **PA**. $E°'_a$ and $E°'_b$ is the pH-dependent formal potential for the phenol with deprotonated and protonated carboxylic acid group, respectively. *b)* Scheme of the pH-dependent potentials for the case where $pK_a(COOH)_{red} < pK_a(COOH)_{ox}$.

Employing this scheme relies on the assumption that pK_a(COOH) is the same for the reduced and oxidized form of the compounds. However, this is not true, necessarily, since H-bonding and conjugation of the H-bond and COOH-group might affect the pK_a upon oxidation. To investigate the magnitude of the pK_a change, in paper **IV** DFT calculations were used to estimate $pK_a(COOH)_{ox}$ and $pK_a(COOH)_{red}$, using the correlation between O-H bond lengths and vibrational frequencies for series of substituted benzoic acids of known pK_as.[c] The result, shown in Table 1, is that the calculated $pK_a(COOH)_{ox}$ is only 0.4 and 0.2 units higher for **SA** and **PA**, respectively, than the measured value of that in the reduced form. With this small correction taken into account the difference in driving force for the CEP reaction **Ru**-**SA** and **Ru**-**PA** is 0.27 V, with a slightly uphill reaction for the **Ru**-**SA** and a downhill path for the **Ru**-**PA** (Table 1). Note that the subsequent deprotonation of the COOH group in **Ru**–**SA** is rapid and will drive the reaction to completion.

The thermodynamic treatment above is not sufficient in itself for analyzing the competition between the separate PCET mechanisms. Other parameters, like reorganization energy and vibronic coupling, are also important. The following sections will explore also these parameters from the kinetics, starting with the pH-dependence of the rate.

4.2 Kinetics and mechanisms

There are some studies in the literature that explore the mechanism of PCET in the kinetics of phenol oxidation and influence from H-bonded bases, but the solution conditions and methods used vary. Electrochemical oxidation of phenols by cyclic

[c] The details of these calculations were explained in the supplementary information of in paper **IV**.

voltammetry is advantageous in that one can control the potential for the oxidation and is used together with simulations of the voltammograms[106-108] and by indirect oxidation of phenol via a metal complex oxidant[109,110]. The interpretation might be complicated, however, since the conditions for charged species near the electrode are different than in solution due to the difference electric field strength.[108] Also, due to the high phenol concentrations often used the local pH will change upon release of the proton to low buffered media.[111] Spectroscopic methods are also used together with stopped-flow techniques[102,112-114] and by time-resolved emission[115,116]. In the present thesis laser flash-quench method is used, monitoring the absorption changes (described in chapter 3). For **Ru-SA** and **Ru-PA** this allowed for *direct* determination of the rate constants, without influence of diffusion steps or simulations of electrochemical data. Thus, paper **III** and **IV** are the only comprehensive studies, known in literature so far, that contain mechanistic studies on PCET from unimolecular systems in water solutions. In the complementary study in paper **I**, the bimolecular reaction between $[Ru(bpy)_3]^{3+}$ and **SA**, **PA**, ***p*-SA** and ***p*-PA** was measured under pseudo-first order conditions in phenol concentration, giving k'. The second order rate constant was then calculated from $k_{obs} = k'/[PhOH]$.

The pH-dependence of the observed rate constants, in Figure 11, shows a marked difference for the H-bonded phenols and non-H-bonded reference compounds. For the intramolecular systems (Figure 11a) the covalently linked analogue, **Ru-Y** (Figure 14 in Ch. 5) is used as a non-H-bonding reference. The proton in this is released directly to the bulk and thus gives a pH-dependent PCET rate constant.[d] In contrast, for **Ru-SA** and **Ru-PA** the rate constant is pH-independent the range where H-bonding is possible, i.e. $pK_a(COOH) < pH < pK_a(OH)$. The same trend is observed for the bimolecular reactions in Figure 11b. Thus, the rate constant within this pH range is assigned to a PCET with proton transfer to the H-bonding base, k_{HB} (Table 2).

For PCET reactions it is generally not difficult to decide whether or not it is a PCET since the reactants and products can usually be observed experimentally. The difficulty is rather to determine through which path the reaction proceeds. But to be able to do this, experimental markers, like potentials, rate constants and kinetic isotope effects, are needed. These are used in the further discussion to compare the mechanistic routes that may be responsible for the observed PCET reaction.

[d] Part of this thesis and former work (ref. 125,126,132) contain somewhat surprising results showing that the concerted PCET from phenols with a proton release directly to water bulk, is weakly pH-dependent, and not to be explained by the OH^- or another base accepting the proton. This has emerged in a quite extensive debate and a section in the following chapter 5 will spent discussing this.

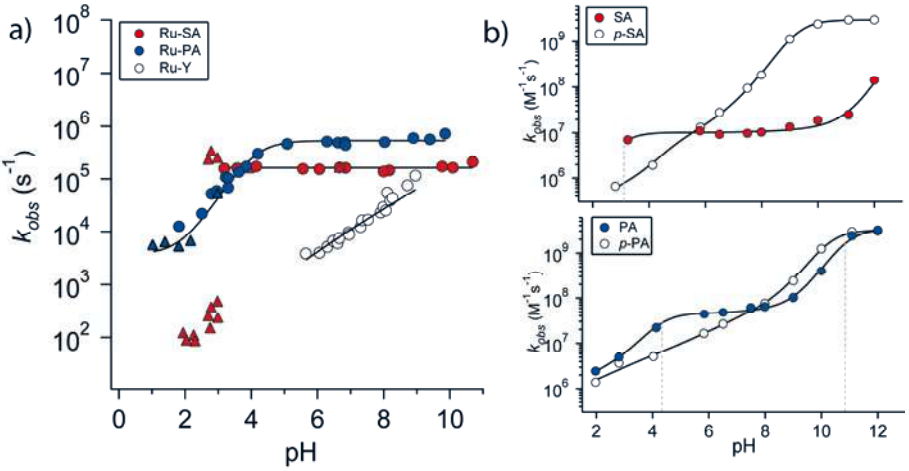

Figure 11. *a)* The rate constant of the phenol oxidation in the intramolecular systems vs. pH. The solid line for **Ru-PA** is a fit to eq. 20. The rate constant were measured using either MV^{2+} (circles) or $[Co(NH_3)_5Cl]^{2+}$ (triangles) as external quencher (see Ch. 3). Details of conditions can be found in SI of paper **III**. *b)* The pH-dependence of the second order rate constants for oxidation of the substituted phenols, **SA**, ***p*-SA**, **PA** and ***p*-PA**, calculated from the pseudo first order rate constant (paper **I**). For details of the fitting, see paper **I**. k_{HB} obtained from the fits are given in Table 2.

Table 2. Output parameters for fitting the data in Figure 11, and kinetic isotope effects.

	k_{HB}	k_H/k_D (pH/pD = 6 or 7)
Ru-SA	1.6×10^5 s^{-1}	1.9
Ru-PA	5.2×10^5 s^{-1}	2.7
SA	1.0×10^7 $M^{-1}s^{-1}$	1.2
PA	4.3×10^7 $M^{-1}s^{-1}$	1.6
***p*-SA**	-	2.1
***p*-PA**	-	2.1

For an intramolecular PTET with a reversible deprotonation/protonation prior to the electron transfer step the observed rate constant should be equal to eq. 19:

$$k_{obs} = k_{PT1} \times k_{ET2} / (k_{-PT1} + k_{ET2}) \qquad (19)$$

Two extreme conditions can be considered for this. Either the reverse PT step is much slower than the subsequent ET step ($k_{-PT1} << k_{ET2}$) giving an observed rate constant equal to that for deprotonation: $k_{obs} = k_{PT1}$. This is, however, unlikely. First, the reverse protonation step from a strongly acidic group to a strongly basic group is very fast: $k_{-PT1} = 6\times10^{12}$ s^{-1}, as expected within a H-bonded complex given by Eyring equation. Secondly, the expected k_{PT1} can be calculated from the equilibrium constant which in turn is given by the difference in pK_a values for the OH and COOH groups: $k_{PT1} = 10^{-\Delta pK_a} \times k_{-PT1}$. With a $\Delta pK_a = 10.4$ for **Ru-SA** this would give a $k_{PT1} = 2\times10^2$ s^{-1} which is far below the observed rate constants. This first case can

thus be excluded as the mechanism for **Ru-SA** and **Ru-PA**. The other extreme case would be an ET limited reaction, $k_{-PT1} >> k_{ET2}$. The observed rate constant is then given by the electron transfer rate constant times the fraction of the phenolate form: $10^{-\Delta pK_a} \times k_{ET2}$. To account for the observed rate constants, k_{ET2} would need to be in the picosecond time regime which much larger than $k_{ET} = 5\times10^7$ s^{-1} observed for oxidation of the PhO^- form in **Ru-Y** (discussed in Ch. 5). These estimates show that a PTET mechanism is not consistent with the data. Similar arguments can be used for the bimolecular reactions (see paper **I**).

In the ETPT mechanism, the initial endergonic ET step will be rate limiting. The subsequent deprotonation of $PhOH^{\bullet+}$ within the H-bond is very fast, $k_{PT2} = 6\times10^{12}$ s^{-1}, since the pK_a of this species is ca. -2. Therefore, the observed rate constant for ETPT will be equal to the rate constant for the ET1, $k_{obs} = k_{ET1}$. The relative rates of bimolecular systems **SA**, ***p*-SA**, **PA** and ***p*-PA** should then correlate with the $PhOH^{\bullet+}$/PhOH potentials. However, in paper **I** it is described that such a correlation does not exist for these compound.

From the kinetic arguments the stepwise mechanisms are excluded. Instead, PCET from the H-bonded phenols is assigned to a CEP mechanism. We saw from the thermodynamic treatment above that both the stepwise mechanisms involve endergonic first steps while the second step is fast and exergonic. The power of this second step is instead put into the overall driving force for the CEP mechanism. This will therefore benefit from having a strong base as proton acceptor and a more acidic proton on the phenolic group. This is consistent with the larger k_{HB} observed for **PA** which has a smaller ΔpK_a than **SA**. Similar trends have been demonstrated by others in intermoleculary H-bonded phenols.[110,117] However, as calculated from eq. 18, $\Delta G°_{HB}$ is ca. 0.27 eV more favorable for **Ru-PA** than for **Ru-SA** (Table 1), which should result in roughly 2 orders of magnitude difference in k_{HB} for the two compounds. However, the observed difference is much smaller, for which the answer is to find in the other parameters, i.e. reorganization energy or the coupling constant. It has been observed in phenol with intramolecular N-bases that the rate is increased for phenols with resonance assisted H-bonds (RAHB). This effect was explained by the decrease in λ upon strengthening of the H-bond for the conjugated systems.[113,114] In contrast to our systems the nature of the base was not crucial. Even though **SA** has a RAHB and **PA** not, the increased magnitude in k_{HB} for **SA** is not explained by a stronger H-bond. The H-bonding energy is, in fact, smaller in **SA** than **PA**, determined from DFT calculations below. As the Marcus equation is too simple to explain the small difference in rate constants, the following discussion will present a modified Marcus model which not only manage to explain this difference but also suggests what the important parameters for CEP reactions are.

The pH-dependence of the rate constants for the bimolecular reactions was discussed in detail in paper **I**. Briefly; the observed rate constant for ***p*-SA** and ***p*-PA** could not be fitted with a first order dependence on OH^- or buffer and was instead fitted with a

pH-dependent rate constant (discussed in Ch. 5). We suggest that this is due to the deprotonation to the bulk water. Note that this is different from the pH-dependent k_{obs} observed for **Ru-PA** at low pH, discussed next.

4.3 H-bond gating

Interestingly, for **Ru-SA** and **Ru-PA** the rate constants observed at pH < 4 (in paper **III**) revealed two disparate pH-dependences. For **Ru-SA**, as the pH is lowered and approaches pK_a(COOH) the amplitude of k_{obs} drops in magnitude. This is due to breaking of the H-bond as the COOH group becomes protonated. This non-H-bonded fraction, instead, reacts with a 3 order of magnitude slower PCET rate constant (k_w) at these low pHs since the proton is released to the bulk water. Interestingly, the PCET from this fraction in SA gives a pH-dependent k_w, which is in agreement with a deprotonation to the bulk, as observed for **Ru-Y** at neutral pH. The overall observed rate has biexponential kinetics around the pK_a of COOH with pH-dependent titration of the relative amplitudes. The mechanism is shown in Scheme 4 where the formation of the H-bond (k_d) is much slower than k_w. The two fractions therefore react independently, consistent with biexponential kinetics.

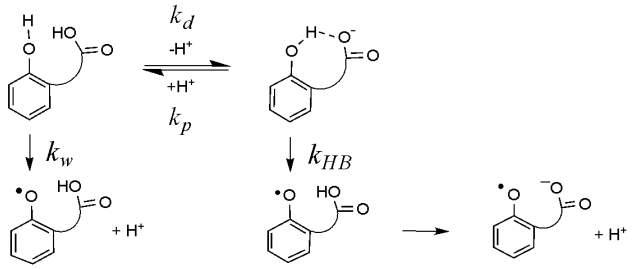

Scheme 4. Mechanistic routes for H-bond gated PCET.

For **Ru-PA**, instead, the kinetics are single exponential at all pH values with an observed rate constant that decreases at pH < 4. In contrast to **Ru-SA**, this is consistent with a rapid H-bond breaking/formation equilibrium where all species react via the fast route, namely via the PhOH···COO$^-$ form. This gives pre-equilibrium kinetics with the observed rate constant equal to:

$$k_{obs} = (1-x)\cdot k_w + x \cdot k_{HB} \qquad (20)$$

where x is the H-bonded fraction given by $(1 + 10^{pK_a(COOH) - pH})^{-1}$. The **Ru-PA** data in Figure 11 is fitted to equation 20, giving a pK_a of ca. 4.3 which is in perfect agreement with the measured pK_a(COOH) of **PA**.

The flexibility of the H-bond needs not to be correlated with the H-bond strength. The DFT calculations below resulted in a weaker H-bond for **SA**, still the kinetic data suggest that it has a less flexible H-bond. This may be because the H-bond in SA is resonance assisted, which gives the C–C bond and the C–O more double bond character. A possible reason could therefore be that this makes the

rotation around these bonds harder and therefore the 6-ring in **SA** more stiff than the 7-membered ring in **PA**.

4.4 Numerical modeling of temperature-dependent rate (paper **IV**)

There has been much debate over which parameters contribute to the large variations of the rate using different hydrogen bonding proton acceptors. One factor might be the reorganization energy which should be smaller in ET than in a bidirectional CEP, since the movement of the surrounding nuclei in response to the transfer of the positive charge requires additional energy. Another important parameter is the overlap of the proton vibrational wave functions in the reactant and product state, i.e. the proton coupling term. These two factors will contribute differently to the temperature-dependence of the rates because λ appears in the exponential term while the proton coupling term is found in the pre-exponential factor of the Marcus rate expression. The proton coupling term will give a large contribution to the KIEs since the proton vibrational wave function is largely dependent on the isotope, while the exponential term is expected to be mostly independent on isotope. This section presents an in-depth analysis of temperature data and kinetic isotope effects (KIE) using the Kuznetsov-Ulstrup model[118]. This model includes *promoting vibrations*, which modulate the proton donor-acceptor distance in the transfer coordinate. These are important in many reactions because they allow the system to achieve significantly larger vibrational wave function overlaps. While this model makes certain simplistic assumptions, most notably that all proton transfers are purely non-adiabatic (even at very short transfer distances), it has been shown to compare favorably to a more explicit model which includes partially and fully adiabatic transfers as well,[119] and donor-acceptor compression within this model gives rise to very similar effects as more explicit calculations of the vibronic couplings in simple model systems[90]. The model has proven very successful in the past for enzyme data.[76,120,121]

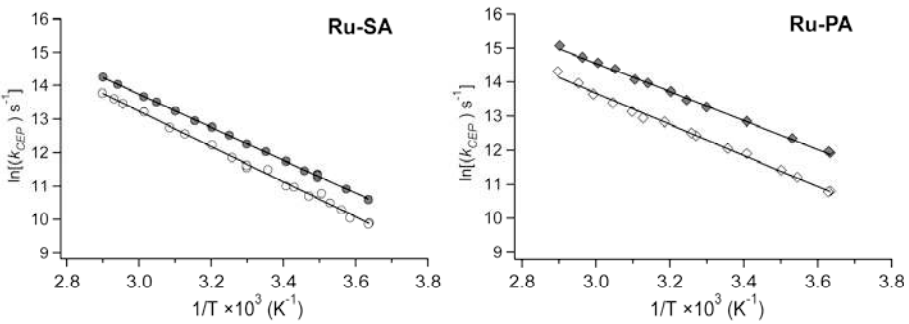

Figure 12. Temperature dependence of k_{HB} at pH/pD = 7 for **Ru-SA** (*left*) and **Ru-PA** (*right*) in H_2O (solid symbols) and D_2O (open symbols). Solid lines are linear Arrhenius fits of the data.

Table 3. Experimental parameters extracted from linear Arrhenius fits (equation 21) of the data in Figure 12.

	Ru-SA		**Ru-PA**	
	H_2O	D_2O	H_2O	D_2O
k_{CEP} (298 K, s^{-1})	1.6×10^5	8.6×10^4	4.8×10^5	1.7×10^5
E_a (kJ mol^{-1})	40.9	43.8	35.2	37.9
A ($\times10^{12}$, s^{-1})	2.38	4.1	0.69	0.75
$V_{\mu\nu}$ (cm^{-1})	106	142	60	63
k_H/k_D (298 K)	1.88		2.78	
ΔE_a (kJ mol^{-1})[I]	2.9		2.7	

[I] $\Delta E_a = E_a(\mathrm{D}) - E_a(\mathrm{H})$

The temperature dependence of bimolecular rate constants is complicated due to the diffusion of the reactants, which in itself is temperature dependent. However, this problem is eliminated for unimolecular systems like **Ru-SA** and **Ru-PA**. Thus, k_{HB} and kinetic isotope effect at pH/pD = 7 were measured over a wide range of temperatures (2−70°C) for these complexes. Figure 12 and Table 3 summarize the kinetics and the parameters extracted from a linear Arrhenius fit with a Marcus pre-exponential factor (equation 21).

$$k_{CEP} = A\exp\left(-\frac{E_a}{RT}\right) \qquad A = \frac{1}{2\pi}\left|V_{\mu\nu}\right|^2\sqrt{\frac{4\pi^3}{\lambda RT\hbar^2}} \tag{21}$$

The linear Arrhenius equation (21) is a simple version of the modified model used in eq. 22 below for numerical modeling of the data in Figure 12, and which includes transitions to and from vibrational excited states and a proton vibrational wavefunction overlap term. The latter is largely affected by the presence of promoting vibrations. As a comparison the data were modeled both with and without the incorporation of promoting vibrations for which the results will be discussed below. The numerical modeling procedure is exhaustively described in paper **IV** and will not be fully repeated here. Only a brief description will be presented as well as the most important results and conclusions.

This model is based on the complete rate expression:

$$k_{CEP} = \sum_{\mu} P_\mu \sum_{\nu} \frac{1}{2\pi}\left|V_{\mu\nu}\right|^2\sqrt{\frac{4\pi^3}{\lambda RT\hbar^2}}\exp\left(-\frac{\left(\Delta G^\circ + \Delta E_{\mu\nu} + \lambda\right)^2}{4\lambda k_B T}\right) \tag{22}$$

The exponential term consists of the Marcus parameters, $\Delta G°$, which is the CEP reaction driving force calculated according to the method described in § 4.1.2 and λ, which is fitted. $\Delta E_{\mu\nu}$ is the energy difference between the reactant state, μ, and product state, ν, where both ground and excited vibrational states of the transferring proton are considered. The parameters that describe the reactant and product vibrational wave functions (ϕ_μ and ϕ_ν, resp.), which are the O-H dissociation energy and vibrational frequency assuming Morse potential, were extracted from DFT

calculations. A precise value of these appeared not to be crucial for the results. In the pre-factor, P_μ is the Boltzmann distribution over the phenolic proton vibrational states in the reactant and $V_{\mu\nu}$ the vibronic coupling term. Based on the ET distance and electronic properties of **Ru-Y**, a system very similar to **Ru**-**SA** and **Ru**-**PA**, the ET reaction was expected to be electronically nonadiabatic[122]. In addition the coupling terms obtained in Table 3 is below the limit of ~200 cm^{-1} for nonadiabatic reactions.[90] Thus, the CEP reaction from **Ru**-**SA** and **Ru**-**PA** are treated as nonadiabatic and the vibronic coupling term can be described as:[90]

$$V_{\mu\nu} \approx V_{ET} \left\langle \phi_\mu \middle| \phi_\nu \right\rangle \tag{23}$$

where V_{ET} is the electronic coupling and the bracketed term is the proton coupling term that is the overlap between the vibrational wave functions for the states μ and ν. V_{ET} is expected to be very similar for **Ru**-**SA** and **Ru**-**PA**. Therefore, $V_{\mu\nu}$ informs on the relative strength of the proton coupling. The proton vibrational wave function overlap is strongly dependent on the proton tunneling distance and on the isotope. Compared to electrons, protons have much more localized wave functions due to the greater mass, making PT very sensitive to the tunneling distance. Therefore, vibrations that cause the proton donor-acceptor distance to decrease will increase the tunneling probability and cause the majority of CEP events to occur over shorter distances than the equilibrium distance. These are the so called *promoting vibrations*.

4.4.1 Promoting vibrations

A promoting vibration is here modeled as a classical harmonic oscillator that modulates the donor-acceptor (D−A) distance, and therefore the H^+/D^+ tunneling distance, illustrated in Figure 13. At equilibrium separation of D−A the tunneling distance is r_0. The promoting vibration compresses D−A with a distance, r_X, generating a new tunneling distance, Δr. The promoting vibration is characterized by its force constant (k_X) which gives the energy $E_X = ½ r_X^2 k_X$. The nuclear wave function overlap at temperature T is then the integral of the overlap term for all possible values of Δr, weighted by their respective population:[118]

$$\left\langle \phi_\mu \middle| \phi_\nu \right\rangle = \int_{\Delta r=0} \left(\delta\Delta r \left\langle \phi_\mu \middle| \phi_\nu \right\rangle_{\Delta r} \frac{\exp(-E_X/k_B T)}{\int_{\Delta r=0} \exp(-E_X/k_B T)} \right) \tag{24}$$

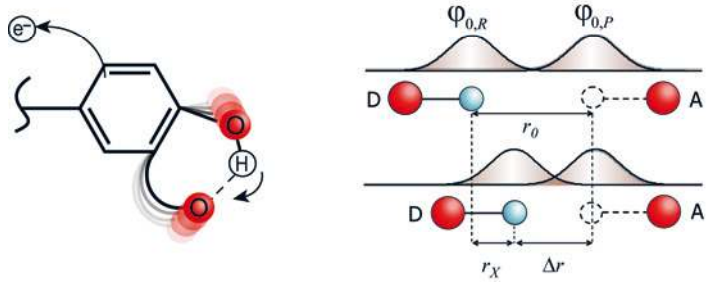

Figure 13. Schematic picture of promoting vibrations and the increased effect it has on the proton vibrational wave function overlap.

For the numerical modeling of the data in Figure 12 there are only three variable parameters that are modified during the fitting, while there are four independent experimental observable to which the model is fitted in equation 22. These observable are k_{CEP}, E_a, ΔE_a and KIE (at 298 K), while the independent parameters are V_{ET}, λ and k_X. The fixed input parameters determined from other independent methods are r_0, $\Delta G°$ and the parameters that describe ϕ_μ and ϕ_ν. The general procedure for reproducing the experimental data using equation 22 was a three step method as follows:

(1) k_X is modified until the experimental value of KIE at 298 K is reproduced.
(2) λ is modified until the activation energy E_a is matched with the experimental value in Table 3.
(3) V_{ET} is modified until $k_{CEP(H)}$ at 298 K is the same as the experimental value.

The results are given in Table 4. As a comparison the data was also modeled without promoting vibrations using a fixed tunneling distance. In this attempt for first step (1) in the general procedure above the wave function overlap in equation 24 is not integrated over several Δr, but instead kept constant ($\Delta r = r_0$) while the r_0 is varied to reproduce the experimental KIE. This approach led to a significant change in the output values as the data in Table 4 display.

Table 4. Best-fit parameters for modeling of data in Figure 12 using eq. 22 – 24.

	Ru-SA		**Ru-PA**	
	fixed Δr	with pr. vib.	fixed Δr	with pr.vib.
r_0 (Å)	0.23	0.6	0.29	0.6
k_X (J m^{-2})	–	11.9	–	21.2
λ (kJ mol^{-1})	148	132	173	153
V_{ET} (kJ mol^{-1})	2.64	4.90	2.56	3.82

The equilibrium PT distances where estimated from molecular models (DFT) for the reactant and product state of **SA** and **PA**, using the O−O distance and the O−O−H angle in the reactant and product. The O−O distance was somewhat shorter in **SA** than in **PA** (2.52 Å and 2.59 Å resp.) and the H-bond angle (O−H···O) is more linear in **PA** than in **SA** (167.1° and 154.7° resp.) which resulted in almost identical PT distances for the compounds: 0.62 Å for **SA** and 0.63 Å for **PA**. Thus, a value of

0.6 was used for r_0 in the modeling *with* promoting vibrations. For the modeling *without* promoting vibrations, a r_0 = 0.23 Å for **Ru–SA** and r_0 = 0.29 Å for **Ru–PA** was required. This is significantly shorter than the equilibrium distance determined from DFT calculation above, suggesting that D–A fluctuations are necessary to shorten the tunneling distance. Moreover, the values obtained for λ is in agreement with promoting vibrations. It was carefully described in paper **IV** that the reorganization energy for these types of systems is not expected to exceed 130 kJ mol^{-1}, partly based on DFT calculations for λ_i. The value for λ of 132 and 153 kJ mol^{-1} from a variable Δr in the modeling is more in agreement with this estimate.

The H-bond strength was estimated from DFT calculations simulations by rotating the O–H group away from the COOH group. Surprisingly, the H-bond energy was always smaller for **SA** for all the levels of theory used. This means that even though **SA** has a shorter O–O distance and a resonance-assisted H-bond the fact that it has a more bent H-bond dominates over the other properties in affecting the H-bond strength. However, the slightly weaker H-bond for **SA** is in agreement with the smaller value of k_X obtained from numerical modeling. This means that **SA** has a *softer* H-bond mode which makes the promoting vibration more facile, thus giving shorter tunneling distances. It is often assumed that shorter H-bonds are equal to stronger H-bonds, which might apply to very similar H-bond where all other parameters are equal, **SA** and **PA** provides a simple example of the opposite. That points to the importance to distinguish between *short*, *strong* and *stiff* hydrogen bonds. The softer promoting vibration in **Ru-SA** compensates to a larger extent for the lower driving force and thus decreases the difference of rate constant.

The promoting vibrations increase the wave function overlap from about 2% to 20% for **SA** and to 10% for **PA** (where $<\phi_\mu|\phi_\nu> = 1$ for $\Delta r = 0$). This is because the majority of the PCET reactions occur at 0.2–0.3 Å, which is significantly shorter than the equilibrium D–A separation,[e] concluding that promoting vibrations are indeed important, and is an additional parameter that should be included to model CEP reactions more accurately. Dynamical effects from the environment has been used before to model proton tunneling events in enzymes[8,88,123] and in unidirectional PCET in amidinum-carboxylate salt-bridge complexes.[116] The effects from promoting vibrations are seen in the magnitude of KIE and the rate constants. For our systems it was calculated that k_{HB} will be over a magnitude smaller if the proton was tunneling from the equilibrium distance. The KIEs was also calculated to ca. 40 for fixed Δr = 0.6 Å. The modest KIEs observed for many PCET reactions can be explained by the presence for promoting vibrations.

[e] The distribution of rates are for **Ru–PA** peaking around 0.30 Å for H and 0.24 Å for D, and for **Ru–SA** they peak around 0.22 Å for H and 0.18 Å for D, as shown by Figure 8 in paper **IV**.

4.5 Conclusions

Two very similar H-bonded phenols are compared. This allows for a fine-tuned study on effect on PCET from variation in the H-bond. At pHs where H-bonding is possible, i.e. pK_a(COOH) < pH < pK_a(OH), k_{obs} is pH-independent for (**Ru-**)**SA** and (**Ru-**)**PA**, in contrast to the non-H-bonding reference compounds: ***p*-SA**, ***p*-PA** and **Ru-Y**. This is assigned to a PCET with deprotonation to the H-bonding base. From kinetic and thermodynamic arguments the stepwise ETPT and PTET mechanisms are excluded for this, leaving CEP as the only possible alternative.

In previous studies on bimolecular PCET from phenols, the rate was correlated mainly with the driving force, which is determined primarily by the pK_a of the base.[102,110,113] In another comparison of three phenols with internal N-bases it was instead concluded that the key feature is the RAHB in the phenol which give stronger H-bond resulting in larger rate constant due to smaller λ, while the nature of the base is not critical.[114] For the phenols studied here, we conclude that the difference in rate constant cannot be explained only by the difference in pK_a, but also by additional effects due to difference in H-bonds.[f]

Detailed analysis by numerical modeling of the data for **Ru-SA** and **Ru-PA** led to several findings: (1) Promoting vibrations need to be incorporated in the model to explain the data accurately. (2) Shorter D-A distance does not necessarily mean a stronger H-bond. The linearity of the H-bond is also important. (3) PCET oxidation of phenol does seem to involve significant inner reorganization energy, but this can be lowered if PT occurs via short hydrogen bonds. (4) RAHB does not necessarily mean a stronger H-bond. The RAHB in **Ru-SA** facilitates the PCET reaction, not because of stronger H-bonding as suggested for similar compounds,[114] but due softer promoting vibration. Moreover, the nature of H-bond in **SA** is apparently making the bonding/breaking of the H-bond more difficult compared to **PA**. This is observed at pH < 4 where the rate constant for **Ru-SA** and **Ru-PA** shows two disparate pH-dependencies, consistent with an H-bond gating mechanism.

[f] Note that a good H-bonding agent is not the same as a strong proton acceptor. The latter is expressed by the pK_a which affect the thermodynamics, while a short H-bond will affect the rate by increasing the proton vibrational overlap and reducing the reorganization energy.

5 PCET from phenols with external proton acceptors

This chapter will deal with PCET from phenols that lack an intramolecular H-bonding base and for which either the water solvent or another external base act as the primary proton acceptor. The pH-dependent kinetics of phenol oxidation in *bimolecular* reactions is dominated by the phenolate fraction (paper **I**).[111,124] Here we present oxidation rates from a phenol that is covalently linked to the electron acceptor. This is, to my knowledge, the only example where PCET is studied within a linked model system in aqueous solution. A new pH-dependence was observed for this,[125,126] that was not first-order in [OH^-], and that is heavily debated.[109,127,128] What is the origin of this pH-dependence? Can OH^- or the base form of the buffer act as primary proton acceptors and give this pH-dependence? These questions will be discussed here together with the possible mechanistic paths for PCET. Moreover, this simple model molecule can be modified by substituents which tune the redox properties of the compound. This opens up for a competition between the different PCET mechanisms and which has led to the finding of four different intramolecular oxidation mechanisms within the same type of molecule: ETPT, CEP, PTET and pure ET, making it valuable on a fundamental level for PCET theory.

5.1 Background

The model compound, discussed first in this chapter, consists of a $[Ru(bpy)_3]^{2+}$ part which is covalently linked to a tyrosine via a amide bridge, **Ru-Y.**[129] Oxidative quenching of the photoexcited Ru-part generates the neutral tyrosyl radical in a subsequent step (see Ch. 3 and Figure 14). pH-dependent kinetic studies on **Ru-Y** were first published in 2000 and show two discrete rate constants: one slower that is pH-dependent and one faster that is pH-independent (open black circles in Figure 14).[126] When pH ≈ pK_a of the tyrosine the kinetics are biexponential with relative amplitudes depending on pH. The faster rate constant at pH > 10, was thus attributed to a pure ET from tyrosinate while the slower rate constant below pH = 10 was recognized as PCET from the protonated tyrosine, as was supported by the difference in E_a: 0.32 eV and 0.05 eV for PCET and ET, respectively. Due to the significant kinetic isotope effect of 2.0–2.5 observed at pH < 10 it was suggested that the PCET from phenol occurs via a CEP mechanism. In addition, within this pH range (5 < pH < 9), all other mechanisms could be excluded, as will be discussed in the following sections.

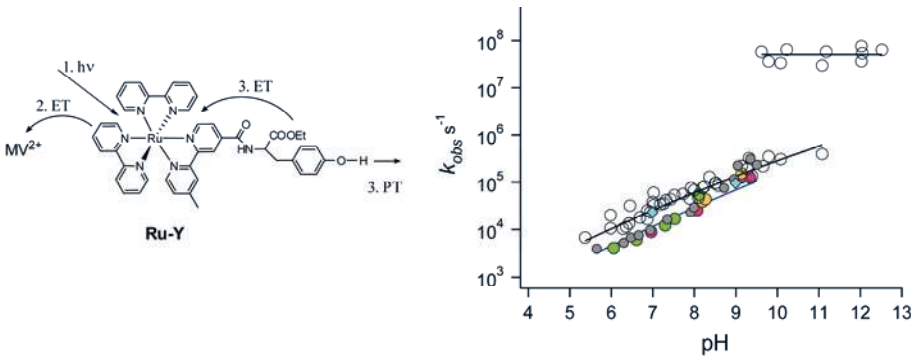

Figure 14. *Left:* Scheme of the reaction steps in **Ru-Y**: the photo-induced quenching (1-2) and PCET reaction (3). *Right:* pH-dependence of k_{obs} in **Ru-Y** in 10 mM (○) and 0.5 mM (●) phosphate/borate mixture, at 0.5 mM buffer concentrations with MES (●, pK_a = 6.2), borate (●, pK_a = 9.1) and phosphate (●, pK_a = 7.2) and in neat water(◆). The solid lines are fits to Marcus equation (eq. 8 and 26) (pH < 10) or a zero slope line (pH > 10).

The observed pH-dependence raises the question whether it is the solvent molecule that is the primary proton acceptor or if it is the basic form of the buffer. Therefore, in paper **II**, the rate constant was measured in different buffer concentrations, showing that the base form of phosphate, HPO_4^{2-}, is the primary acceptor only at high enough concentrations, as will be discussed later in this chapter. At buffer concentrations below 5 mM the rate is independent on buffer concentration. In this range the buffer base is outcompeted by another proton acceptor, presumably H_2O. Still, the data exhibits the same dependence on pH as was observed in ref. 126. This is shown by the colored symbols in Figure 14, where the rate constant is measured at 0.5 mM concentration in several buffers. Even though it is very hard to control the pH in non-buffered solution, especially around pH 7 where the buffer capacity of water is the worst, the rate constants obtained in pure water was also pH-dependent. The data in buffered and non-buffered solution span the same range of rate constants over the pH range ca. 3−9. The experimental data show that the pH-dependence is real, however, but it is not clear what the origin of this pH-dependence is. This will be discussed in the following sections.

5.2 Water and OH^- as proton acceptor

With a p$K_a \approx$ -1.7 for H_3O^+, the water molecule is a poor proton acceptor. But as any water molecule is part of the of bulk, involved in the H-bonded network, it might not be correct to consider the isolated water molecule as the proton accepting base, but rather a collective action by the surrounding water cluster. As discussed in chapter 2 and pointed out by others, the solvation of H^+ with just one water molecule is insufficient.[64,65,68] At least a few water molecules should be involved and aligned in a proper configuration for the proton transfer to occur. Although the microscopic picture for deprotonation of phenols to water is complex and might be beyond the scope of this thesis, the experimental data point to a picture that is more intricate than just the single water molecule model. Note that the observed pH-dependence is

very different from that for deprotonation of Eigen acids. The rate is usually pH-dependent and determined by the pK_a of the acid: $k_{PT} \approx 10^{11-pK_a}$ s^{-1}.

Another potent proton acceptor would be the hydroxide ion. Although it exist in very low concentrations at neutral pH it is a very strong base (pK_a(H_2O) = 15.7) and should be considered. Especially for weaker acids and a high pH the deprotonation may instead become first order in [OH^-] (Scheme 5).

The following sections we present expected rate constants and pH-dependences for the stepwise and concerted mechanisms, considering both H_2O and OH^- as single proton acceptors (Scheme 5). This leads us to exclude the stepwise mechanisms and instead propose the CEP as the mechanism.

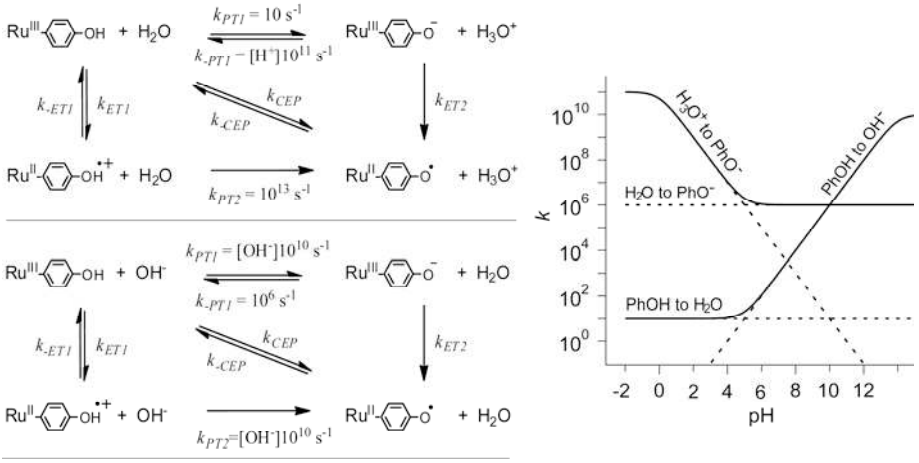

Scheme 5. *Left:* The stepwise ETPT and PTET mechanisms in the corner reactions and the concerted mechanism shown in the diagonal reaction with either H_2O (upper) or OH^- (bottom) as proton acceptor. *Right:* The calculated forward and backward PT rates vs. pH.

5.2.1 PCET via a ETPT mechanism

As the pK_a for $PhOH^{+\bullet}$ is ca. −2, it will release its proton to the aqueous medium within a few picoseconds,[67] independently of the proton acceptor (H_2O or OH^-). Therefore, the ETPT reaction will be ET-limited with k_{obs} equal to k_{ET1} in Scheme 5. This is not expected to depend on either the pH or buffer concentration and was accordingly excluded as the mechanism for the data below pH 9 in Figure 14. In addition, k_{ET1} should correlate with $E°_{PhOH^{+\bullet}/PhOH}$ and give small kinetic isotope effects. The significant KIE of 4.5 observed in 0.5 mM buffer concentration at pH 7 is not consistent with an ETPT mechanism.

5.2.2 PCET via a PTET mechanism

First, let us consider PTET mechanism with OH^- as proton acceptor (left bottom panel Scheme 5). Applying a steady-state approximation gives an observed pseudo-first order rate constant $k_{obs} = [OH^-]k_{PT1}\cdot k_{ET2}/(k_{-PT1} + k_{ET2})$. Two limiting conditions can be considered: (1) $k_{ET2} << k_{-PT1}$ gives $k_{obs} = [OH^-]k_{ET2}\cdot k_{PT1}/k_{-PT1}$ that depends on

the pK_a of TyrOH: $k_{obs} = [OH^-]k_{ET2}\cdot 10^{14-pK_a}$. For **Ru-Y**, this case can be excluded because the condition does not hold. $k_{ET2} = 5\cdot 10^7$ s^{-1} measured for the phenolate oxidation at pH > 10 (Figure 14) while $k_{-PT1} \approx 10^6$ s^{-1} estimated from pK_a value of PhOH. (2) The other limiting case where $k_{-PT1} << k_{ET2}$ will be limited by the first PT step giving $k_{obs} = [OH^-]k_{PT1}$. For a diffusion limited deprotonation to OH^- ($k_{PT1} \approx 1\cdot 10^{10}$ M^{-1}s^{-1})[67] the rate constant becomes $1\cdot 10^3$ s^{-1} at pH 7 (Scheme 5), which is too slow to explain the observed rate at that pH ($k_{obs} \approx 1\cdot 10^4$ s^{-1}). Moreover, PTET in both limit (1) and (2) will be first-order in $[OH^-]$ giving a slope of 1 in the log k vs. pH plot and cannot explain the weaker slope of 0.4−0.5 observed for **Ru-Y** in Figure 14.

If instead H_2O is the proton acceptor the pre-equilibrium treatment gives $k_{obs} = k_{PT1}\cdot k_{ET2}/(k_{-PT1} + k_{ET2})$ and we can again use the two limiting assumptions: (1) For $k_{ET2} << k_{-PT1}$ the proton transfer depends on the pK_a for tyrosine, $k_{obs} = 10^{-pK_a}\cdot k_{ET2}$ and therefore we would not expect a pH-dependence at all. In addition, to account for the observed rate constant at pH 7, we would get the unphysical value of $1\cdot 10^{15}$ s^{-1} for k_{ET2}. (2) For the opposite case ($k_{-PT1} << k_{ET2}$) the observed rate constant is just equal to that for deprotonation to H_2O ($k_{obs} = k_{PT1}$), which for tyrosine is very small: ~10 s^{-1} [67] at all pHs. To summarize, PTET to H_2O would not be dependent on pH at all and would give much smaller rates than observed in Figure 14.

5.2.3 PCET via a CEP mechanism

As for the PTET, CEP with OH^- as proton acceptor will also be first-order in $[OH^-]$ giving a slope of 1 on the log k vs pH plot. In contrast to exergonic PT between Eigen acids,[68] CEP is activated. Moreover it involves an ET component with weak coupling, V_{ET} (see chapter 2). The diffusion controlled encounter between tyrosine and OH^- will therefore be the upper limit for the expected rate constant giving $k_{obs} \leq 10^{10}\cdot[OH^-]$ s^{-1}. This applies for the irreversible CEP.

If we continue to consider the water molecule as a single accepting base but also consider the reverse step (−CEP) the expected overall rate constant becomes the sum of the forward and backward rate: $k_{obs} = k_{CEP} + k_{-CEP}\cdot[H_3O^+]$. This gives a rate constant that *decreases* with pH and clearly does not explain the data in Figure 14. Furthermore, this equilibrium treatment should only be relevant for small driving forces where the forward and backward rate becomes similar. That would be at ca. pH 1 for **Ru-Y**. Instead, with a $\Delta G°$ = -0.4 at pH 7 for **Ru-Y**, the backward rate cannot not compete with the forward rate and the rate that we observe directly is k_{CEP}. Thus, a CEP mechanism to a proton accepting water molecule is expected to be pH-independent as well since the $[H_2O]$ does not change noticeably with pH. This has been pointed out by others[84,128] and used as an argument that CEP reactions with water as proton acceptor is in general pH-independent.

None of the mechanistic treatments above are predicts the mild pH-dependent rate constant observed 5 < pH < 9 in Figure 14, the stepwise mechanisms are not

consistent with the observed pH-slope, magnitude of rate or kinetic isotope effect and are therefore excluded. Moreover, the data can not be explained by a CEP reaction where a single molecular species act as the proton acceptor in the rate-determining step. In any case, the high kinetic isotope effect and high E_a were arguments for a CEP mechanism in ref. 125. The high E_a was interpreted by Sjödin et al. as caused by a high λ for CEP. The new data, measured in lower buffer concentrations give even higher KIE (4.5) and E_a (0.46 eV), see Table 5. These values are strong indications that the reaction proceeds via a concerted mechanism.

5.3 The pH-dependence of the rate constant

Redox potentials can be obtained experimentally by electrochemical methods that measure the PhOH ⇆ $PhO^{\bullet} + H^{+}$ overall equilibrium. This gives a Nernstian behavior of $E^{\circ}_{PhO^{\bullet}/PhOH}$ with a slope of 59 mV per pH unit at pH < pK_a as illustrated in Figure 15 and eq. 25.

$$E^{\circ}_{PhO^{\bullet}/PhOH} = E^{\circ}_{PhO^{\bullet}/PhO^{-}} + 59\text{mV}\cdot\log(1+10^{pK_a - pH}) \quad (25)$$

$$\Delta G^{\circ}_{CEP} = -F(E^{\circ}_{Ru^{III/II}} - E^{\circ}_{PhO^{\bullet}/PhOH}) \quad (26)$$

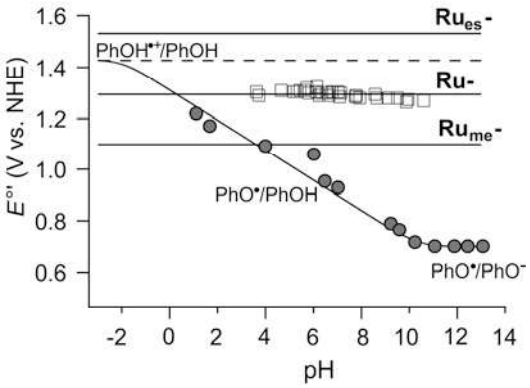

Figure 15. pH-dependent redox potentials of $Ru^{III/II}$ for the three compounds (**Ru_{es}-Y**, **Ru-Y** and **Ru_{me}-Y**, see below) and TyrOH and with the pH-dependent driving force indicated. Data for PhOH and $Ru^{III/II}$ are reprinted from ref. 130.

Sjödin et al. suggested that the observed pH-dependence of the rate constant is due to a Marcus-type free-energy dependence, using ΔG°_{CEP} as in eq. 26. They noted, however, that it is not clear how this elementary reaction senses the pH-dependence of $E^{\circ}_{PhO^{\bullet}/PhOH}$ that is due to the mixing entropy of the released proton. It is predicted by Marcus theory that for small driving forces ($\Delta G^{\circ} < \lambda$) a change by ca. 120 meV in ΔG° gives one order of magnitude difference in rate constant, i.e. 0.5 slope on the log k vs pH plot. Thus, with the pH-dependent ΔG° in eq. 26 and a fixed λ obtained independently from temperature measurements at pH 7, data in Figure 14 was nicely fitted.[130]

It has been discussed that the activation energy for an elementary process within a precursor/successor complex should only depend on the reactants and not on the concentration in solution.[131] It was thus claimed that using a pH-dependent driving force in the Marcus activation energy is not appropriate,[128] and the data in ref. 126 was put into question.[109,127] However, it was shown by Sjödin et al. that correlation of the 0.5 slope in the log k vs. pH plot and 59 mV change of $\Delta G°$ per pH unit is phenomenological. Apparently, the rate constant is correlating with a pH-dependent driving force in a Marcus fashion. It remains, however, to be elucidated if this is coincidental or if the factors determining the rate dependence on pH are connected to the overall free energy.

In paper **I** we reported that the bimolecular reaction between phenol and $[Ru(bpy)_3]^{3+}$ is pH-dependent with the similar slope as observed for the linked compound, **Ru-Y**. k_{obs} was not a simple titration between phenol and phenolate. Instead a pH-dependence in the rate constant had to be included. However, the bimolecular rate constant was measured at 100 mM buffer concentrations and it has to be cleared out whether it is not the buffer causing this pH-dependence for these. The second order rate constant was difficult to measure with significant accuracy at lower buffer concentrations. Instead, we test here if the observed pH-dependence can be explained by a reaction with buffers. Thus, the data for the para-substituted phenols are fitted to a model assuming that HPO_4^{2-} is the primary acceptor (eq. 27) in Figure 16. In equation 27 the only parameters that vary with pH are the fractions of the respective species (α). The rate constants for PCET to HPO_4^{2-} ($k_{HPO_4^{2-}}$), PCET to water (k_w) and ET from phenolate (k_{PhO^-}) are held constant in the fit. The separate terms are indicated by the dashed lines in Figure 16. Obviously, fitting eq. 27 to the data gives a bad fit at pH < 6 and a simple titration of the phenol and buffer is not sufficient to explain the observed pH-dependence.

$$\alpha_{PhOH} \cdot (\alpha_{HPO_4^{2-}} \cdot k_{HPO_4^{2-}} \cdot [\text{Phosphate}] + k_w) + \alpha_{PhO^-} \cdot k_{PhO^-} \qquad (27)$$

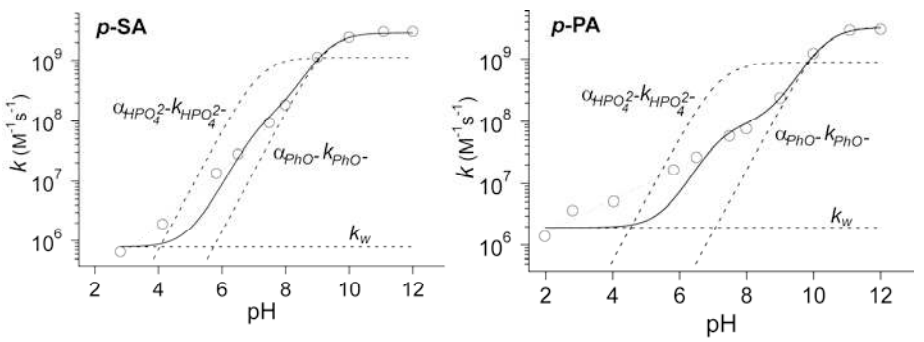

Figure 16. The pH-dependent data for ***p*-SA** and ***p*-PA** fitted to eq. 27 (solid line). The dashed lines illustrates the different fractions of k_{PhO^-}, $k_{HPO_4^{2-}}$ and k_w.

5.4 Four mechanistic regions (paper **V**)

The data for **Ru-Y**, discussed so far, showed two different regions: one at pH > 10 which was attributed to a pure e^- transfer from tyrosinate, and one at ca. 5 < pH < 9, identified as a concerted e^-/H^+ transfer to H_2O. In a more recent, expanded study using a larger pH range and 0.5 mM buffer two new regions appear (Figure 17): one pH-independent range at pH < 5 (region A), and one at ca. 9 < pH < 10.5 which has a steeper dependence on pH (region C). The data below pH 10 switches smoothly between the separate regions, indicating that this is a competition amongst different PCET mechanisms rather than a new molecular form reacting. The latter case could give a biexponential rate, and jump in magnitude if the rate constants largely deviate, as is seen for the rate constants of the Ru-TyrOH and Ru-TyrO$^-$ fractions. Instead the rate constant is single exponential at pH below ca. 10 and changes continuously with the fastest mechanism dominating at the apparent pH.

$$k_{obs} = k_1 + k_2 \cdot 10^{0.5\mathrm{pH}} + k_3 \cdot 10^{\mathrm{pH}} \qquad (28)$$

The solid line in Figure 10 is a fit to a sum of three rate constants (eq. 28): one pH-independent dominating at low pH (A), one at intermediate pH which has a slope 0.5 (B) and one at high pH which has a slope 1(C). The separate contributions are marked by the dashed lines. Note that the dashed line representing the fraction dominating in region C deviates more than 1 order of magnitude from the data in region B. Correspondingly, a linear fit with slope 1 cannot reproduce the data at intermediate pH. The separate mechanistic regions will now be discussed in the following sections.

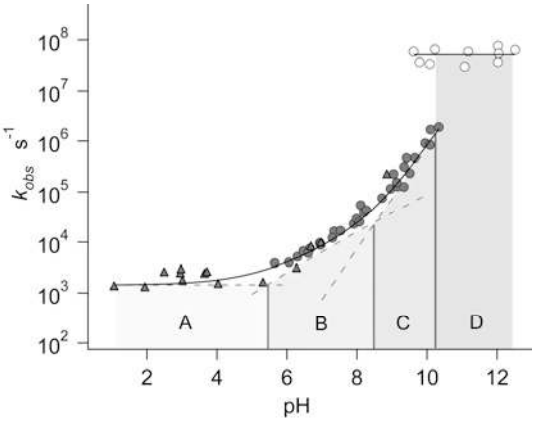

Figure 17. pH dependence of the PCET rate constant for **Ru-Y** in 0.5 mM buffer (solid symbols). and from data in ref. 126 (○). Circles and triangles represents data measured with different external acceptors (methyl viologen and $[Co(NH_3)_5Cl]^{2+}$, resp). Regions A - C is a fit to a sum of three rate constants with slope 0, 0.5 and 1 respectively, each separately represented by a dashed line (eq. 28).

Table 5. Kinetic isotope effects and activation energies.

		Ru_{me}-Y		**Ru-Y**		**Ru_{es}-Y**	
Region	assigned mechanism	k_H/k_D	E_a (eV)	k_H/k_D [b]	E_a (eV)	k_H/k_D	E_a (eV)
A	ETPT	[a]	[a]	2.0	0.44	2[c]	0.26
B	CEP	[a]	[a]	4.5	0.46	> 10[c]	0.60
C	PTET	[a]	[a]	5.5	0.38	–	–

[a] not measured yet, [b] measured at 298 K [b] from ref. 130

5.4.1 Region C: PTET to OH^-

It was discussed in §5.2 that OH^- is a very strong base but due to its low concentration a neutral pH it, apparently, can not compete with H_2O. At high pH, though, the situation becomes different. A slope 1 of the data in region C is in agreement with a rate that is first order in OH^- concentration, consistent with $k_{obs} = [OH^-]\cdot k_{OH^-}$. The data fitted to this model yields a $k_{OH^-} = 7.3\times10^9$ s^{-1}. This is consistent with a diffusion limited proton transfer to OH^- which is expected to be ca. 1×10^{10} M^{-1} s^{-1}.[65] Thus, the mechanism at high pH is assigned to a PTET to OH^-.

Moreover, the KIE observed at pH/pD 9.5 (Table 1) is also in agreement with this mechanism. As KIEs in this thesis are measured by replacing the entire solvent with D_2O the KIE will not only be affected by H/D-isotope of the phenolic proton but also by the properties of OD^- and OH^-. Autoprotolysis of heavy water is less than of H_2O ($K_w(H) \approx 7.5\cdot K_w(D)$)[70] and the diffusion controlled encounter with OD^-/OH^- will give rise to an apparent isotope effect due to smaller $[OD^-]$ at a certain pD/pH. A KIE = 5.5 is close the expected value of 7.5 and therefore in agreement with a diffusion limited PT to OH^- as the dominating mechanism in region C.

5.4.2 Region A: switch to ETPT

At pH < 5 k_{obs} levels out to a pH-independent rate constant. Note that this is not due the use of $[Co(NH_3)_5Cl]^{2+}$ as an external quencher instead of MV^{2+}, since identical k_{obs} values are obtained at pHs where both can be used. A pH-independent rate constant is consistent with an ET-limited ETPT mechanism, as the low KIE = 2.0 was observed at pH 3. Small or negligible effects from deuteration are expected for pure electron transfers when the entire solvent is exchanged and KIEs < 2 are not unusual.[84] The observed KIE in region A is also remarkably smaller than that observed for the CEP mechanism at pH 7 and would speak to a switch of mechanism.

A pH-independent rate constant and KIE = 2.0 was assigned to an ET-limited ETPT mechanism for a similar compound, bearing a stronger oxidant: **Ru_{es}-Y** (Figure 18).[130] The driving force for the initial ET step is slightly exergonic ($\Delta G°_{ET}$ = -0.07 eV) for this compound, compared to +0.20 eV for the corresponding reaction step in **Ru-Y**. It was interpreted by Sjödin et al. that the preference for ETPT over

CEP using a stronger oxidant originates from the smaller λ for ET. This becomes important only when the $\Delta G°_{CEP}$ is small, i.e. at low pH, and one might expect a switch of CEP to ETPT going from high to low pH. The same situation may be true for **Ru-Y**. Since the ET step is more endergonic than for **Ru$_{es}$-Y**, the k_{ETPT} is smaller and apparently the switch occurs at lower pH. In support for an ETPT mechanism at low pH the next section will show how the rate constant is changed when modifying the potential of the electron accepting species and consequently the $\Delta G°$ for ETPT, in yet another compound.

The extended pH range for PhOH oxidation in **Ru-Y** further demonstrates what a PTET to OH^- or ETPT would look like and thus excludes these as the mechanism in region B. The regions are well separated by the change in slope and the significant difference in KIE. We cannot rule out a pH-independent CEP at low pH, however, but that would require an explanation for the existence of two different CEP mechanism with different KIE and pH-dependence. In contrast to most of the PCET studies on phenols, this is investigated in water solvent and shows a complexity and a richness of PCET from phenols. It shows that a mechanism may be identified, but the situation can change drastically when the conditions are slightly varied. This is because the sensitivity to the conditions of parameters determining the magnitude of the separate paths varies between the mechanisms.

5.5 Switching mechanism by varying the oxidant strength

There are examples in the literature where the use of a strong oxidant is favouring the ETPT mechanism. **Ru$_{es}$-Y** was mentioned above and a few more will be discussed below. Increasing the oxidation power of the oxidant will increase the driving force for both CEP and ETPT. It was suggested by Sjödin et al. that ETPT will be more favoured by this change due to a smaller λ for ETPT than for CEP.[130,132] A change in $\Delta G°$ for reactions with small λ will have a larger impact on the rate constant than for reactions with large λ. Thus, this is seen in the competition between CEP and ETPT using different oxidants.

In paper **I**, $Br^•$ was used as an oxidant of phenol the driving force was 0.35 V more favourable than with $[Ru(bpy)_3]^{3+}$. This led to a rate constant that was independent on pH, as expected for ETPT. The rate showed the expected dependence on the $PhOH^{•+}$/PhOH potential, which was not the case with $[Ru(bpy)_3]^{3+}$. Another example in the literature is the direct oxidation of tyrosine by a photoexcited Re-complex, **Re(P-Y)**.[115] With a potential of 1.78 V vs. NHE for the $Re^{I*/0}$ couple the driving force is increased by 0.52 eV compared to $[Ru(bpy)_3]^{3+}$.

Also this has a pH-independent rate constant within the pH range measured (Paper **II**).[g]

In Figure 18 the structure of three similar compounds are shown. They all cary the same tyrosine in one end but have a Ru-part that is modified by either methyl groups (**Ru$_{me}$-Y**) or ester groups (**Ru$_{es}$-Y**) on the bpy ligand. The only property affecting the PCET rate that should differ between the compounds is the redox potential of the $Ru^{III/II}$ couple. A potential of 1.53 V vs. NHE[130] for the **Ru$_{es}^{III/II}$** couple makes it a 0.27 eV better electron acceptor than $[Ru(bpy)_3]^{3+}$ in **Ru-Y**. Hence, the PCET rate constant is pH-independent in the main pH-range, but, interestingly, it is pH-dependent at pH > 8 (Figure 18). The lack of this pH-dependent phase in D_2O yielded an apparent KIE > 10, suggesting a switch to CEP mechanism at high pH. Moreover, the E_a was treated as a Marcus activation energy (eq. 8) where $\Delta G°$ is given by eq. 26, which yielded λ = 1.2 eV at pH 3 and 2.4 eV for the high pH mechanism. It was interpreted that small λ is a signature for a ETPT, while larger λ are obtained for the CEP mechanism.

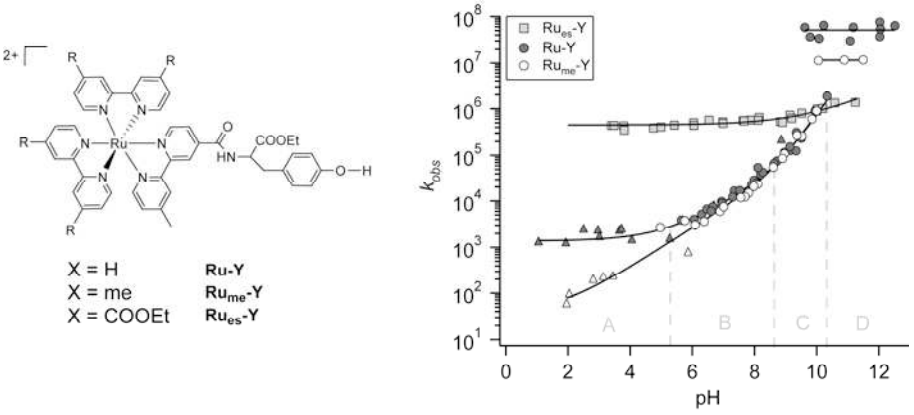

Figure 18. *Left*: Scheme of the structures *Right*: Rate constants vs pH-dependent. The rate constants were measured using either MV^{2+} (circles and squares) or $[Co(NH_3)_5Cl]^{2+}$ (triangles) as external quencher (see Ch. 3).

Ru$_{me}$-Y, has a weaker electron acceptor with a **Ru$_{me}^{III/II}$** potential of ca. 1.10.[133] This gives a 0.16 eV less driving force than $[Ru(bpy)_3]^{3+}$. The data for this shows qualitatively the same dependence on pH as for **Ru-Y**. The Ru-TyrOH and Ru-$TyrO^-$ fraction in **Ru$_{me}$-Y** react independently with biexponential kinetics around pK_a of TyrOH, as for **Ru-Y**. The rate constant at pH > 10 for ET from phenolate is smaller for **Ru$_{me}$-Y** than for **Ru-Y**, as expected for the smaller driving force. The relative rates agree very well with that calculated from eq. 8 based on the different $\Delta G°$ values. The kinetics for the Ru-TyrOH fraction are almost the same

[g] First it was observed that the rate constant was pH-dependent, but was later revised (paper **II** and references therein) as this was measured in 10 mM phosphate buffer concentrations and could instead be assigned CEP to HPO_4^{2-} acting as the primary base. In non-buffered solutions, however, the rate constant was independent on pH. This is discussed in the following sections.

but is continuously pH-dependent at low pH. Interestingly, the switch to ETPT is not seen for this compound. Apparently, with a small driving force the CEP is outcompeting ETPT in a larger pH range. The relative difference in ETPT rates for **Ru_{es}-Y** and **Ru-Y** correlate well with predicted free-energy dependence in eq. 8. The predicted ratio of the rate constants, based on the $\Delta G°$ values, is $10^{2.4}$ while the observed is $10^{2.5}$. Eq. 8 also predicts that the k_{ETPT} = 43 s^{-1} which should give a switch at ca. pH 2, just outside the measured region.

In addition, the switch from CEP to PT-limited PTET to OH^- is also seen for this compound. Noteworthy is that **Ru-Y** and **Ru_{me}-Y** has the same k_{obs} in the C region which is a further proof of a PT-limited PTET with OH^- as primary acceptor, since that is not expected to depend on the oxidation strength of compound. More puzzling is the almost negligible difference in rate in region B. The difference of 0.16 eV in $\Delta G°$ between **Ru-Y** and **Ru_{me}-Y** should give an observable difference of the rate constants. A clear difference in pH-dependent CEP rate constants is instead observed in **Ru_{es}-Y** and **Ru-Y**, which is illustrated in Figure 4c in paper **V**. Although the difference is a factor of ca. 8 it is expected from eq. 8 to be at least 2 orders of magnitude as the $\Delta G°$ deviates with 0.27 eV between the two compounds. These observations speak for a smaller sensitivity of CEP with oxidation strength than predicted before.[130] This is a strong argument against a Marcus-type dependence of the CEP rate on the overall $\Delta G°$ (eq. 26). On the other hand, the much faster rate in **Ru_{es}-Y** shows that rate is not governed by the same limiting factors in all three compounds. The reason for this behavior is to this point not understood and has to be investigated further. The present new data is hoped to help elucidating the origin of the pH-dependence of the CEP reaction.

5.6 Buffer as proton acceptor

We have seen that the PCET reactions occur by parallel mechanisms with H^+ transfer to solvent molecules at conditions where the buffer is absent or in low concentration and not acting as the primary proton acceptor. But many bases may be good candidates as primary proton acceptors. For example, phosphate with pK_a = 7.2 for the $H_2PO_4^-/HPO_4^{2-}$ couple makes PT to HPO_4^{2-} thermodynamically more favourable with ca. 0.5 eV compared to PT to a single H_2O. Thus, at high buffer concentrations and high pH, i.e. conditions where the [HPO_4^{2-}] is large, the dominating pathway is via PCET with H^+ release to the buffer base (paper **II**). This might either occur via PTET or CEP,[109,110] as discussed below.

Figure 19 plots k_{obs} for the three systems, **RuY**, **Ru_{es}-Y** and **Re(P-Y)**, as a function of phosphate concentration and pH. The rate constant increases linearly with base at high concentrations and was fitted to eq. 29 where $1/(1+10^{pK_a-pH})$ is the fraction of the base form, k_b is the second order rate constant for the reaction with HPO_4^{2-} and k_w is the rate constant with water as proton acceptor, given by the intercept in the plots at zero concentration.

$$k_{obs} = k_w + 1/(1+10^{pK_a-pH}) \cdot [\text{Buffer}] \cdot k_b \quad (29)$$

In a similar study[109] the bimolecular rate constant for phenol oxidation with $[Os(bpy)_3]^{2+}$ as oxidant and HPO_4^{2-} as proton acceptor, was measured under saturating condition by electrochemical methods. This yielded an unusually high complexation constant, K_C, for phenol and HPO_4^{2-} and concluded that the reaction went via a PTET within this complex. In the present study we never reach saturating conditions in limit of solubility of phosphate. The discrepancy might lie in the methods as the electric field or the particular coated electrode used in ref. 109 might give an enhanced effect on the complexation between phenol and charged species. In paper **II**, we excluded PTET because the calculated k_{PTET} was smaller than the observed rate, k_b for **Ru-Y**. In addition, because of the similar ΔpK_a of phenol and phosphate measured in H_2O and D_2O, PTET is not consistent with the observed kinetic isotope effect of ca. 2 for **Ru-Y** and 3.0 for **Re(P-Y)**. Also, for the reaction with tyrosine in **Re(P-Y)** with imidazole and pyridine, the measured k_b is much larger than expected for a PTET mechanism, as explained in detail in Supplementary info for paper **II**. An ETPT mechanism should not be dependent on buffer concentration and was therefore also excluded.

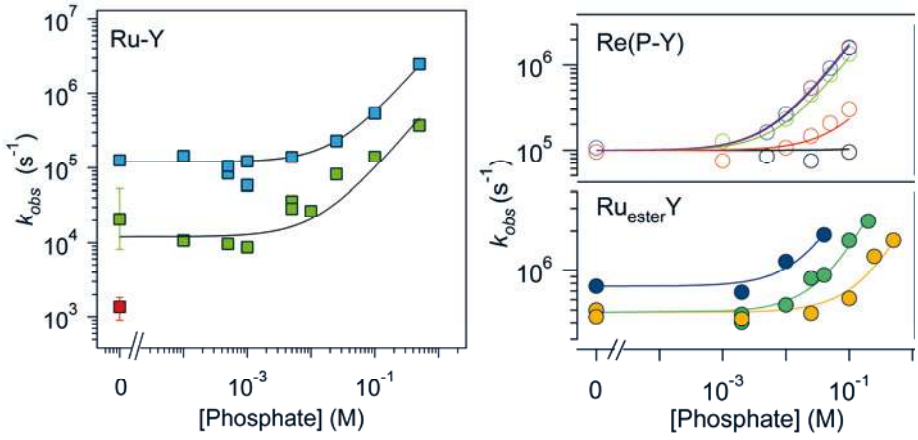

Figure 19. *Left:* Phosphate buffer dependence of k_{obs}, for **Ru-Y** and fits to eq. 29 at pH 7 (■,—), pH 9 (■,—) and pH 3 (■). *Top right*: Phosphate buffer dependence of k_{obs} with fits to eq. 1 for **Re(P–Y)** at pH 4.5 (○), 6.1 (○), 7.5 (○), 8.3 (○), and 9.2 (×). *Bottom right*: Same experiment with **Ru$_{es}$-Y** at pH = 9.9 (●), 7.7 (●) and pH = 6 (●).

On the basis of the discussion above the stepwise mechanisms was excluded. Instead we assigned the mechanism to a CEP with e^- transferred to the metal oxidant and H^+ to the basic form of the buffer. Buffer-assisted CEP is thermodynamically more feasible the stronger base the proton acceptor is, and k_b is therefore enhanced as the pK_a of the base increases (eq. 11 in Ch. 2). This is shown in studies on the bimolecular reaction from phenols H-bonded to pyridines.[117] For **Re(P-Y)**, the dependence of the tyrosine oxidation rate on the concentration of three separate imidazoles could also be correlated with the pK_a of the imidazoles (SI of paper **II**). Another study where $\Delta G°$ was varied by the pK_a of the base, k_b could be

correlated with a Marcus dependence on free energy, in agreement with a CEP mechanism.[110] The correlation might, however, not always be that simple, as shown in chapter 4. Other effects, like for example the strength, length and flexibility of the H-bond between the base and the phenolic group affects the rate significantly. We showed that for the intramolecular H-bonded phenols CEP is facilitated by promoting vibrations which increase the proton coupling term. The H-bond strength has apparently also an effect on λ and shape of the proton-transfer potential for phenols with intramolecular N-bases.[113,114]

5.6.1 Tuning the pK_a of phenol (not published)

The mechanims of PCET might also be tuned by the pK_a of the phenol. The following example is a 2,3-fluoro-substituted phenol covalently linked to the $[Ru(bpy)_3]^{2+}$ photosensitizer, **Ru-FY** (Figure 20). The pK_a of the phenol to is shifted to 7.8 while the $E°$ for the $PhO^{\bullet}/PhO^-$ couple is increased by 0.16 V compared to a non-substituted phenol.[134] This shift makes the CEP reaction in **Ru-FY** only 0.04 V less exergonic but increases the driving force for PT with ca. 0.13 V. It is shown below that a PTET mechanism is thus favored for **Ru-FY**.

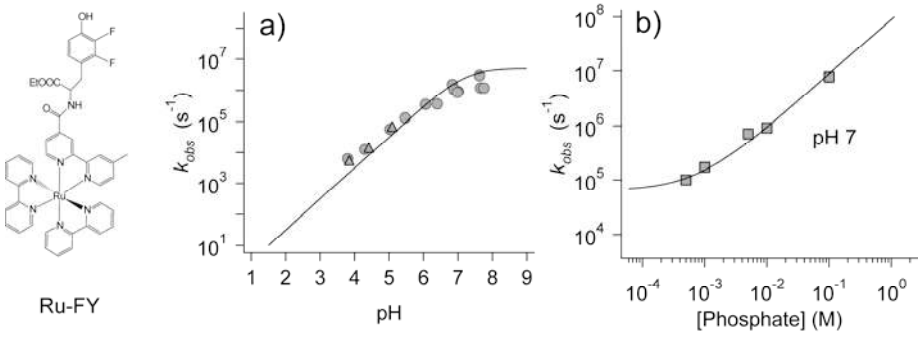

Figure 20. To the left is the structure of **Re-FY**. The observed rate constant for phenol oxidation in **Re-FY** and the dependence on a) pH in 10 mM phosphate buffer and b) on phosphate concentration at pH 7. The solid lines are fits to eq. 29.

As illustrated in Figure 20, the pH-dependent rate constant at pH 7 and in 10 mM phosphate buffer is 2 orders of magnitude faster than for **Ru-Y** at similar conditions (Figure 14). Since the CEP reaction is 0.04 V less exergonic in **Ru-FY**, a CEP to solvent cannot explain this difference. Instead, the pH-dependence follows the titration of HPO_4^{2-}, with a slope of 1 and out leveling at high pH as the pK_a of phosphate is reached. Apparently, HPO_4^{2-} is the primary H^+ acceptor in the whole pH range measured. The fit of the buffer dependence in Figure 20b to eq. 29 gives $k_b = 3\times10^8\ M^{-1}\ s^{-1}$. Using this and the ΔpK_a = 0.6 gives a rate constant for the deprotonation of H_2PO^- by PhO^- equal to $1.2\times10^9\ M^{-1}\ s^{-1}$, which is what is expected for a diffusion controlled reaction between molecules of that size. Thus, the buffer-assisted PCET within **Ru-FY** most likely occurs via a PT-limited PTET mechanim. The much smaller ΔpK_a compared to **Ru-Y** is the reason for the difference. These results provide a simple example illustrating how PTET can be

favored by tuning the pK_a of the phenol. The driving force for PTET changes with 59 mV per pK_a unit determined from the shift in equilibrium constant. However, the change in electronic distribution that substituents induce will usually not only change the acidity of the phenolic proton but also change the electronic properties. This affects the CEP driving force which depends on both properties. In this case these effects counteract and make the CEP less favorable and PTET to dominate.

5.7 Conclusions

Previous reports by Sjödin et al. noted a new type of pH-dependence of the PCET rate constant of phenol oxidation in **Ru-Y**.[126,130,132] This has a slope of 0.5 on the log *k* vs. pH plot and had not been seen before for any other system. The mechanism was assigned to a CEP with deprotonation to water, but has been questioned by others who suggest that buffer of OH^- are the primary proton acceptors.[109,128] Here (paper **II**) we have reinvestigated the pH-dependence of **Ru-Y** in a more extended study where the effects from buffer and OH^- can be excluded. We show that the pH-dependence with a slope of 0.5 is real. The stepwise mechanisms can be excluded, leaving CEP as the proposed mechanism. The significant KIE also supports this.

In addition to previous studies we have found that phenol oxidation within the same molecule, **Ru-Y**, follows four separate mechanisms that dominate in different pH-regions (paper **V**). Firstly, for the Ru-PhO$^-$ fraction dominating at pH > 10 the reaction is a pure ET. Secondly, for the Ru-PhOH fraction three different PCET mechanisms were found. PTET with PT to OH^- at pHs around 10, CEP around pH = 7 and ETPT at pH < 4. Only the CEP and ET from Ru-PhO$^-$ was observed before by Sjödin et al.[126] Interestingly, the relative competition between the mechanisms could be tuned by oxidation strength in **Ru$_{me}$-Y** and **Ru$_{es}$-Y**.

We have shown that at high buffer concentrations the base form of the buffer (e.g. HPO_4^{2-}) may be acting as the primary acceptor depending on pH. For the **Ru-Y** this appeared to be where [buffer] > 5mM. Buffer-assisted PCET from phenol in **Ru-Y** occurs via a CEP mechanism. This is supported by the significant KIE observed for this reaction but also since the magnitude of k_b is not consistent with any of the stepwise paths. However, when ΔpK_a is small, the dominating mechanism is PTET to buffer, as observed of **Ru-FY**. The results show the mechanistic richness and complexity of phenol oxidation, especially when water is the proton acceptor.

6 Final remarks

The systems studied in this thesis have proven to be useful models for proton-coupled electron transfer reactions from Tyr_Z in photosystem II, as they provide similar ET and PT transfer distances and similar redox potentials as the natural system. The possibility of investigating the effects from varying the base and H-bond properties in these artificial systems opens up for suggestions of what the role of H190 in photosystem II is. In the model systems the phenol is covalently linked to a photosensitizer which allows for *direct* determination of the rate constant by flash photolysis experiments. Moreover, as these measurements are done in water this work is a unique study where PCET is measured in a unimolecular system with water as the solvent. How are hydrogen bonds involved in PCET? How does the nature of the proton acceptor affect the PCET reaction? These questions have been addressed.

In the first part, two very similar phenols containing an intramolecular proton acceptor were compared. It was shown that PCET in these occurs via a concerted mechanism. This was based on thermodynamic and on kinetic arguments. In the second part, the proton acceptor was either the water solvent itself or an external base in the buffer. Some of the important conclusions of this thesis work can be summarized in Figure 21. In this the merged pH dependence of k_{PCET} in **Ru-SA**, **Ru-PA** and **Ru-Y** is compared with the pH-dependent rate of Tyr_Z oxidation in PSII.

It was shown in chapter 5 that the oxidation of tyrosine in **Ru-Y** coupled to deprotonation to the bulk is pH-dependent with a slope of 0.5 (Figure 21, labeled B). This mechanism is also consistent with the weak dependence seen for the slowest phase of Tyr_Z oxidation (1). In the Mn-depleted preparations of PSII Tyr_Z is more exposed to the solvent making this a potential proton acceptor. Is has been suggested that the pH-independent phase (2) originates from the fraction that is H-bonded to histidine (H190). This model is supported by the results from our model system. We showed that PT within an intramolecular H-bond does give an pH-independent rate constant that is faster than with neutral water as proton acceptor (B).

The model systems reveal other mechanistic regimes as well. At $pH < pK_a$(base) for **Ru-SA** and **Ru-PA** PCET occurs via H-bond gated mechanisms (F). Depending on the rate for breaking/forming the H-bond, this gives disparate pH-dependencies. For the protonated fraction in **Ru-Y** instead two additional mechanistic regions were observed. One was assigned to a pH-independent ETPT mechanism at low pH (A) and the other to a PTET to OH^- at high pH (C). At $pH > 10$ the phenolate fraction of **Ru-Y** dominates giving a large pH-independent

k_{obs} for the pure ET (D). Note that this is not the same situation as observed for Tyr_Z in the intact PSII (3). Tyr_Z is most likely still protonated and its oxidation is faster than in Mn-depleted PSII probably due to a shorter H-bond that decreases the proton tunneling distance. Moreover, we saw for **Ru-PA** and **Ru-SA** that promoting vibrations further decrease the proton tunneling distance and thus give small KIE. This may also be important for TyrZ oxidation in the intact PSII and is supported by the small KIE. Interestingly this reaction is still active at 5 K where promoting vibrations are not important and support the fact the PT occurs via a short H-bond.

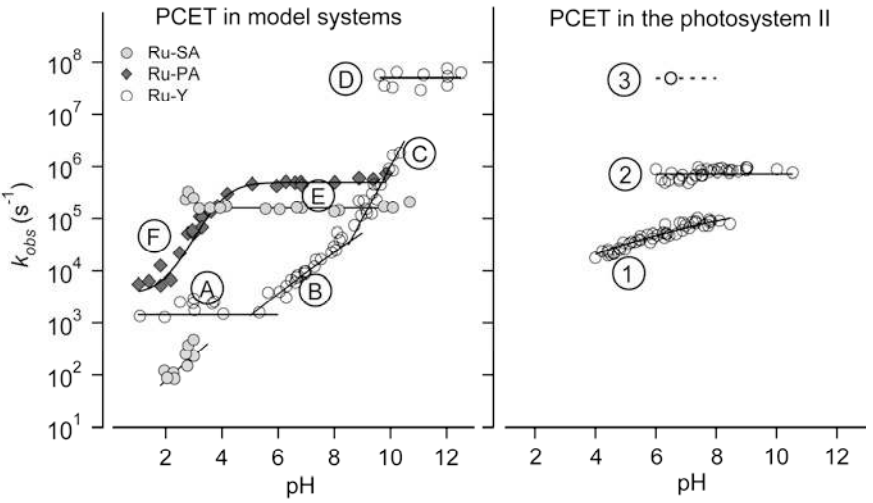

Figure 21. The rate ladder of tyrosine oxidation in water. *Left*: The PCET rate constants vs. pH within the model systems discussed in this thesis. The letters represent the different mechanistic regions for PCET: ETPT with PT to water (A), CEP with PT to water (B), PTET with PT to OH^- (C), pure ET from phenolate (D), CEP with PT to internal H-bond (E) and the region where PCET occurs via H-bond gating (F). *Right*: PCET rate constant for Tyr_Z oxidation in Mn-depleted PSII, region 1 and 2 (reprinted from ref. 35) and in intact PSII[38], region 3.

To summarize, the model systems shows an intricate picture where the competition between the PCET mechanisms may be controlled by pH, proton accepting base or oxidation strength. All these effects should be considered when designing the redox components able to accept or donate protons. I hope that the results in this thesis may contribute and give ideas of how an artificial photosynthesis should be constructed in the future.

Protonkopplad elektronöverföring från vätebundna fenoler

Denna avhandling handlar i huvudsak om att förstå *protonkopplad elektron-överföring* som är ett av alla de elementära reaktionsteg som sker i många biologiska system. Det är viktigt att förstå hur reaktionsstegen i naturliga system sker, särskilt för forskningen inriktad mot *artificiell fotosyntes.*[h] En artificiell fotosyntes är ett konstgjort system som har samma funktioner som den naturliga fotosyntesen; det använder solenergi för att spjälka vatten till syrgas och andra energirika molekyler. Det finns inget sådant idag men hoppet är att det i framtiden ska leda till ett rent och förnyelsebart sätt att omvandla solenergi till ett bränsle, så som t.ex. vätgas.

Den allmänna debatten om världens energikonsumtion har på senaste tiden dragit till sig särskild uppmärksamhet. Det betonas bland annat av att Nobels fredpris 2007 tilldelades IPCC (FN's klimatpanel) och Al Gore för deras arbete för att öka kunskapen om klimatändringar. I skrivande stund pågår klimatmötet i köpenhamn (COP15)[i] där man hoppas kunna ena alla länder i en gemensam plan att bromsa den globala uppvärmingen. Nyligen antog EU-kommissionen det s.k. 20-20-20-paketet[j] vilket innebär att fram till 2020 ska växthusgaserna minska med 20%, att 20% av energin ska vara förnyelsebar och att energiförbrukningen ska minska med 20%. Med andra ord är energidebatten och klimatfrågorna tätt sammankopplade.

Klimatändringar, såsom ökning av växthusgaser, ökning av den globala temperaturen i havet och atmosfären och därefter glaciärsmältning, havsnivå-ökningar etc. är med största sannolikhet en effekt av hur vi människor lever och förbrukar vår energi. Cirka 85% av av vår energiförsörjning kommer idag från fossila bränslen, som olja, kol och naturgas. Det råder inga tvivel om att dessa energikällor så småningom kommer att sina, utan frågan är bara *när?*. Vi måste förr eller senare ersätta de befintliga energikällorna med nya som är miljövänliga och förnyelsebara.

Ett uppenbart alternativ är att använda sig av solenergi. Tillgången är nästintill oändlig. Vi behöver bara veta hur vi ska ta tillvara på den på ett energi- och kostandseffektivt sätt. Solceller är ett alternativ och de är energieffektiva och finns

[h] *Artificiell fotosyntes. Energi från sol och vatten 2008.* Statens Energimyndighet. et 2007:53
[i] en.cop15.dk/
[j] http://ec.europa.eu/climateaction/eu_action/index_sv.htm , www.energimyndigheten.se

ute på markaden. Men kostnaden att tillverka dessa är fortfarande för hög för storskalig produktion. Dessutom producerar solceller elektrisk energi, som är svår att lagra, istället för bränslen. Därför satsas även forskning på andra alternativ, som t.ex. artificiell fotosyntes.

Den naturliga fotosyntesen sker i kloroplatsen i de gröna växternas celler. I denna så livsviktiga process fångas solenergi upp av klorofyllmolekyler i ett första reaktionssteg. Denna energi används sedan i en väl koordinerad kedjereaktion som slutligen leder till att energin binds som kemisk energi. Vidare används denna av celler som bränsle för att bygga ny biomassa. Vatten är den ultimata elektronkällan i dessa reaktioner och som biprodukt bildas syrgas, den syrgas vi använder för att leva. Ett konstgjort system måste liksom det naturliga kunna fånga solljus, skapa ett laddningsseparerat tillstånd, transportera elektroner och de motsvarande "elektron-vakanserna" till var sin katalysator och katalysera en reaktion som t.ex. spjälkning av vatten. Mycket forskning satsas på de olika delarna. Denna avhandling fokuserar i huvudsak på det tredje steget: transporten av elektroner på ett effektivt sätt.

Protonkopplad elektronöverföring är ett av alla de reaktionssteg som sker från det att en ljusfoton träffar ett klorofyll och till dess att en syrgasmolekyl bildas. I det steget separeras, i motsatta riktningar, en proton (en positiv laddad partikel) och en elektron (en negativt laddad partikel) från en och samma molekyl. Vilka parametrar är det som styr att en negativt och en positivt laddad partikel på detta sätt separeras samtidigt? Det är frågställningen i denna avhandling.

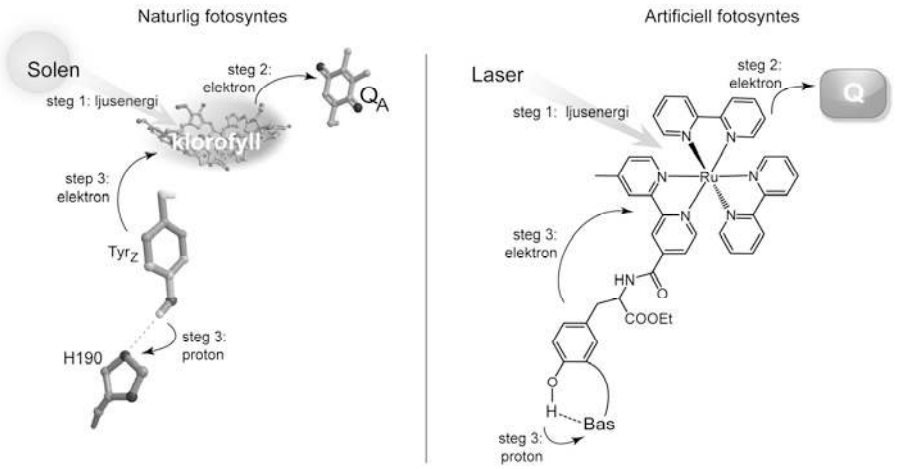

Figur. Schematisk bild över några av de viktiga reaktionssteg som sker i fotosyntesen. 1) Ljusenergi fångas upp av klorofyll. 2) Reaktionskedjan startar med att en elektron hoppar till Q_A. 3) Klorofyllet reduceras av Tyr_Z samtidigt som en proton lämnar Tyr_Z via en vätebindning till H190, i en så kallad *protonkopplad elektronöverföring*. Till höger visas en schematisk bild över modellmolekylen och det reaktionssteg som studeras i denna avhandling.

Som modellmolekyl använder vi oss av en syntetiskt framställd molekyl som liknar några av delarna i det naturliga fotosystemet (se figur). Den består av en *ruteniumdel* som fångar in ljusenergin (och därför imiterar klorofyllet) och en *fenoldel* som innehåller den elektron och proton vi vill studera. I det naturliga systemet

representeras den av aminosyran tyrosin (Tyr_Z). Fenolens OH grupp ingår i en vätebinding till antingen en internt bunden bas eller till en bas i lösningen. I det naturliga systemet är Tyr_Z mer eller mindre permanent vätebunden till en histidin (H190). Basens uppgift är i huvudsak att fungera som en acceptor för protonen. Eftersom protonens rörelse är kopplad till elektronens så kommer karaktären på basen, d.v.s. dess pK_a, påverka drivkraften för elektronöverföringen.

Även vätebindningars behandlas egenskaper i denna avhandling. Vätebindningen fungerar som en transportväg för vätejonen (protonen), och beroende på hur kort, stark och flexibel den är, så påverkar det även den protonkopplade elektronöverföringen.

Vatten är ett medium vars intermolekylära krafter består till största delen av vätebindingar. Vatten har den egenskapen att det kan ta upp protoner och snabbt transportera iväg dem. Bland annat av dessa anledningar har reaktionen studerats i just vatten. Det finns ännu inte många studier som använder vatten som medium för att studera mekanismen för PCET. Dels kan det vara problem med att lösa upp många av de kemiska föreningar man vill studera i vatten, och dels så tillkommer det ett extra komplicerat reaktionssteg att just vattnet självt kan ta upp protonen. Men det är just detta som är en av de saker belyses i denna avhandling. Sedan är vatten det mest naturliga och det medium som man i slutändan bör använda för att producera vätgas i artificiell fotosyntes.

Jag hoppas att resultaten i denna avhandling kan bidra och ge idéer till hur artificiell fotosyntes ska konstrueras i framtiden.

Acknowledgements

I would first like to express my deepest gratitude to my supervisor, Prof. Leif Hammarström, for the scientific guidance, for your eternal enthusiasm and for all the fun we've had on the way! A special thanks to Dr. Martin Sjödin, who co-supervised me during my first years and taught me everything about PCET. I am very thankful for the possibility to collaborate with Dr. Linus Johannissen, for the fruitful scientific discussions and for the help with proof reading this thesis. A major thanks to Dr. Mingtian Zhang, for all the scientific work (synthesis, measurements and preparations), for the PCET discussions, and for your never ending enthusiasm. I would like to give a big thanks to Dr. Olof Johansson for the synthesis of the compounds in paper III. I am very grateful to Dr. Todd Markle who made a major effort in proof reading this thesis and who has helped me with scientific questions. A special thanks to my colleagues overseas, Prof. Dan Nocera and Dr. Steve Reece, for our collaborations and for all the fun we've had! Thanks, Amy Scott, for your experimental contributions in paper V. Great thanks to Prof. Stenbjörn Styring for all the work with the Swedish Consortium and Solar-H and for your enthusiasm and encouragement. I would also like to thank all the people in the Solar-H/H_2 community, especially Prof. Holger Dau, André Klauss and Prof. Ally Aukauloo with group, for our collaborations. I thank my collaborators within the Swedish Consortium and the people at the Fotomol department. Thanks for making my work place a nice and enjoyable place. I also thank CF Liljewalchs resestipendier who granted me with money for conferences.

Finally, and most importantly, I thank my family and friends. Tack mamma och pappa för allt ni ställt upp med och givit mig under dessa år... Mina brorsor, speciellt Darko som hjälp mig med sammanfattningen på svenska och för alla sköna fjällvandringar vi gjort tillsammans. Tack, familjen Schwartz för att ni alltid finns till hands, Inger och Inga-lill för allt ni ställt upp med. Kristin och Viggo för att ni är så sköna kompisar! Laban för att du kom till! Mest av allt, Lennart för din obegränsade kärlek och för att du finns i mitt liv. Tack!

References

1. R. A. Binstead; B. A. Moyer; G. J. Samuels; T. J. Meyer, *J. Am. Chem. Soc.*, **1981**, *103*, 2897.
2. M. Y. Okamura; M. L. Paddock; M. S. Graige; G. Feher, *Biochim. Biophys. Acta.*, **2000**, *1458*, 148.
3. G. T. Babcock, *Proc. Natl. Acad. Sci.*, **1999**, *96*, 12971.
4. J. Stubbe; D. G. Nocera; C. S. Yee; M. C. Y. Chang, *Chem. Rev.*, **2003**, *103*, 2167.
5. C. Aubert; M. H. Vos; P. Mathis; A. P. M. Eker; K. Brettel, *Nature*, **2000**, *405*, 586.
6. G. Litwinienko; K. U. Ingold, *Acc. Chem. Res.*, **2007**, *40*, 222.
7. J. P. Roth; J. C. Yoder; T. J. Won; J. M. Mayer, *Science*, **2001**, *294*, 2524.
8. J. P. Klinman, *Biochim. Biophys. Acta.*, **2006**, *1757*, 981.
9. "International Energy Outlook (2009)" (2009).
10. "IPCC 2007: Summary for policy makers" (2007).
11. J. Barber, *Chem. Soc. Rev.*, **2009**, *38*, 185.
12. N. S. Lewis; D. G. Nocera, *Proc. Natl. Acad. Sci.*, **2006**, *103*, 15729.
13. M. Grätzel, *Nature*, **2001**, *414*, 338.
14. A. Hagfeldt; M. Grätzel, *Acc. Chem. Res.*, **2000**, *33*, 269.
15. D. Noy; C. C. Moser; P. L. Dutton, *Biochim. Biophys. Acta.*, **2006**, *1757*, 90.
16. S. Vassiliev; D. Bruce, *Photosynth. Res.*, **2008**, *97*, 75.
17. J. Barber, *Biochem. Soc. Trans.*, **2006**, *34*, 619.
18. C. Tommos; G. T. Babcock, *Acc. Chem. Res.*, **1998**, *31*, 18.
19. K. N. Ferreira; T. M. Iverson; K. Maghlaoui; J. Barber; S. Iwata, *Science*, **2004**, *303*, 1831.
20. N. Nelson; A. Ben-Shem, *Nat. Rev. Mol. Cell Biol.*, **2004**, *5*, 971.
21. N. Nelson; C. F. Yocum, *Annu. Rev. Plant Biol.*, **2006**, *57*, 521.
22. N. Kamiya; J. R. Shen, *Proc. Natl. Acad. Sci.*, **2003**, *100*, 98.
23. B. Loll; J. Kern; W. Saenger; A. Zouni; J. Biesiadka, *Nature*, **2005**, *438*, 1040.
24. A. Zouni; H.-T. Witt; J. Kern; P. Fromme; N. Krauss; W. Saenger; P. Orth, *Nature*, **2001**, *409*, 739.
25. A. Guskov; J. Kern; A. Gabdulkhakov; M. Broser; A. Zouni; W. Saenger, *Nat. Struct. Mol. Biol.*, **2009**, *16*, 334.
26. H. Dau; M. Haumann, *Coord. Chem. Rev.*, **2008**, *252*, 273.
27. J. Yano; J. Kern; K. Sauer; M. J. Latimer; Y. Pushkar; J. Biesiadka; B. Loll; W. Saenger; J. Messinger; A. Zouni; V. K. Yachandra, *Science*, **2006**, *314*, 821.
28. J. P. McEvoy; G. W. Brudvig, *Chem. Rev.*, **2006**, *106*, 4455.
29. J. Clausen; W. Junge, *Nature*, **2004**, *430*, 480.
30. M. Haumann; P. Liebisch; C. Mueller; M. Barra; M. Grabolle; H. Dau, *Science*, **2005**, *310*, 1019.

31. R. J. Debus; B. A. Barry; I. Sithole; G. T. Babcock; L. McIntosh, *Biochemistry*, **1988**, *27*, 9071.
32. B. A. Diner; R. D. Britt, *Adv. Photosynth. Respir.*, **2005**, *22*, 207.
33. F. Rappaport; J. Lavergne, *Biochim. Biophys. Acta.*, **2001**, *1503*, 246.
34. C. Tommos; G. T. Babcock, *Biochim. Biophys. Acta.*, **2000**, *1458*, 199.
35. R. Ahlbrink; M. Haumann; D. Cherepanov; O. Boegershausen; A. Mulkidjanian; W. Junge, *Biochemistry*, **1998**, *37*, 1131.
36. G. Renger, *Biochim. Biophys. Acta*, **2004**, *1655*, 195.
37. C. W. Hoganson; G. T. Babcock, *Science*, **1997**, *277*, 1953.
38. H. J. Eckert; G. Renger, *FEBS Letters*, **1988**, *236*, 425.
39. A. M. A. Hays; I. R. Vassiliev; J. H. Golbeck; R. J. Debus, *Biochemistry*, **1998**, *37*, 11352.
40. W. Junge; M. Haumann; R. Ahlbrink; A. Mulkidjanian; J. Clausen, *Phil. Trans. R. Soc. Lond. B*, **2002**, *357*, 1407.
41. G. Renger; T. Renger, *Photosynth. Res.*, **2008**, *98*, 53.
42. A. M. A. Hays; I. R. Vassiliev; J. H. Golbeck; R. J. Debus, *Biochemistry*, **1999**, *38*, 11851.
43. M. Haumann; W. Junge, *Biochim. Biophys. Acta.*, **1999**, *1411*, 121.
44. F. Mamedov; R. T. Sayre; S. Styring, *Biochemistry*, **1998**, *37*, 14245.
45. F. Rappaport; M. Guergova-Kuras; P. J. Nixon; B. A. Diner; J. Lavergne, *Biochemistry*, **2002**, *41*, 8518.
46. F. Rappaport; A. Boussac; D. A. Force; J. Peloquin; M. Brynda; M. Sugiura; S. Un; R. D. Britt; B. A. Diner, *J. Am. Chem. Soc.*, **2009**, *131*, 4425.
47. B. A. Diner; J. A. Bautista; P. J. Nixon; C. Berthomieu; R. Hienerwadel; R. D. Britt; W. F. J. Vermaas; D. A. Chisholm, *Phys. Chem. Chem. Phys.*, **2004**, *6*, 4844.
48. T. J. Meyer; M. H. V. Huynh; H. H. Thorp, *Angew. Chem. Int. Ed.*, **2007**, *46*, 5284.
49. A. Magnuson; M. Anderlund; O. Johansson; P. Lindblad; R. Lomoth; T. Polivka; S. Ott; K. Stensjö; S. Styring; V. Sundström; L. Hammarström, *Acc. Chem. Res.*, **2009**, *42*, 1899.
50. J. H. Alstrum-Acevedo; M. K. Brennaman; T. J. Meyer, *Inorg. Chem.*, **2005**, *44*, 6802.
51. J. E. Bullock; R. Carmieli; S. M. Mickley; J. Vura-Weis; M. R. Wasielewski, *J. Am. Chem. Soc.*, **2009**, *131*, 11919.
52. M. W. Kanan; D. G. Nocera, *Science*, **2008**, *321*, 1072.
53. D. G. Nocera, *Inorg. Chem.*, **2009**, *48*, 10001.
54. V. Balzani; A. Credi; M. Venturi, *ChemSusChem*, **2008**, *1*, 26.
55. W. Lubitz; E. J. Reijerse; J. Messinger, *Energy Environ. Sci.*, **2008**, *1*, 15.
56. M. Hambourger; G. F. Moore; D. M. Kramer; D. Gust; A. L. Moore; T. A. Moore, *Chem. Soc. Rev.*, **2009**, *38*, 25.
57. R. A. Marcus; N. Sutin, *Biochim. Biophys. Acta*, **1985**, *811*, 265.
58. J. R. Bolton; N. Mataga; G. McLendon, *Advances in Chemistry Series*, **1991**, *228*, 1.
59. N. Sutin, *Electron transfer reactions in solution: A historical perspective* in *Electron Transfer - from Isolated Molecules to Biomolecules,* (John Wiley & Sons Inc, 1999), vol. 106, pp. 7.
60. R. D. Canon, *Energetics of electron transfer* in *Electron transfer reactions,* (1980), pp. 175.
61. M. D. Newton; N. Sutin, *Annu. Rev. Phys. Chem.*, **1984**, *35*, 437.
62. P. F. Barbara; T. J. Meyer; M. A. Ratner, *J. Phys. Chem.*, **1996**, *100*, 13148.

63. G. L. Closs; J. R. Miller, *Science*, **1988**, *240*, 440.
64. J. M. J. Swanson; C. M. Maupin; H. N. Chen; M. K. Petersen; J. C. Xu; Y. J. Wu; G. A. Voth, *J. Phys. Chem. B*, **2007**, *111*, 4300.
65. M. Gutman; E. Nachliel, *Biochim. Biophys. Acta*, **1990**, *1015*, 391.
66. J. T. Hynes, *Nature*, **1999**, *397*, 565.
67. M. Gutman, *Biochim. Biophys. Acta*, **1995**, *1231*.
68. M. Eigen, *Angew. Chem. Int. Edit.*, **1964**, *3*, 1.
69. A. J. Kresge, *Acc. Chem. Res.*, **1975**, *8*, 354.
70. R. P. Bell, *The Proton in Chemistry* (Cornell University Press, ed. 2, 1973).
71. E. D. German; A. M. Kuznetsov; R. R. Dogonadze, *J.C.S. Faraday II*, **1980**, *76*, 1128.
72. P. M. Kiefer; J. T. Hynes, *J. Phys. Chem. A*, **2004**, *108*, 11793.
73. P. M. Kiefer; J. T. Hynes, *Solid State Ionics*, **2004**, *168*, 219.
74. L. I. Krishtalik, *Biochim. Biophys. Acta*, **2000**, *1458*, 6.
75. G. A. Jeffrey, *An introduction to hydrogen bonding* (Oxford University Press, ed., 1997).
76. M. J. Knapp; K. Rickert; J. P. Klinman, *J. Am. Chem. Soc.*, **2002**, *124*, 3865.
77. A. Kohen; J. P. Klinman, *Chem. Biol.*, **1999**, *6*, R191.
78. J. M. Mayer, *Annu. Rev. Phys. Chem.*, **2004**, *55*, 363.
79. J. M. Mayer; J. Rhile Ian, *Biochim. Biophys. Acta*, **2004**, *1655*, 51.
80. J. M. Mayer; I. J. Rhile; F. B. Larsen; E. A. Mader; T. F. Markle; A. G. DiPasquale, *Photosynth. Res.*, **2006**, *87*, 3.
81. R. I. Cukier; D. G. Nocera, *Annu. Rev. Phys. Chem.*, **1998**, *49*, 337.
82. S. Y. Reece; D. G. Nocera, *Annu. Rev. Biochem.*, **2009**, *78*, 673.
83. C. J. Chang; M. C. Y. Chang; N. H. Damrauer; D. G. Nocera, *Biochim. Biophys. Acta*, **2004**, *1655*, 13.
84. M. H. V. Huynh; T. J. Meyer, *Chem. Rev.*, **2007**, *107*, 5004.
85. C. Costentin, *Chem. Rev.*, **2008**, *108*, 2145.
86. S. Hammes-Schiffer, *Acc. Chem. Res.*, **2001**, *34*, 273.
87. S. Hammes-Schiffer; E. Hatcher; H. Ishikita; J. H. Skone; A. V. Soudackov, *Coord. Chem. Rev.*, **2008**, *252*, 384.
88. S. Hammes-Schiffer; A. V. Soudackov, *J. Phys. Chem. B*, **2008**, *112*, 14108.
89. R. I. Cukier, *J. Phys. Chem. B*, **2002**, *106*, 1746.
90. J. H. Skone; A. V. Soudackov; S. Hammes-Schiffer, *J. Am. Chem. Soc.*, **2006**, *128*, 16655.
91. J. M. Mayer; D. A. Hrovat; J. L. Thomas; W. T. Borden, *J. Am. Chem. Soc.*, **2002**, *124*, 11142.
92. C. Costentin; D. H. Evans; M. Robert; J. M. Saveant; P. S. Singh, *J. Am. Chem. Soc.*, **2005**, *127*, 12490.
93. A. K. Covington; M. Paabo; R. A. Robinson; R. G. Bates, *Anal. Chem.*, **1968**, *40*, 700.
94. B. Durham; J. V. Caspar; J. K. Nagle; T. J. Meyer, *J. Am. Chem. Soc.*, **1982**, *104*, 4803.
95. N. H. Damrauer; G. Cerullo; A. Yeh; T. R. Boussie; C. V. Shank; J. K. McCusker, *Science*, **1997**, *275*, 54.
96. R. J. Watts, *J. Chem. Ed.*, **1983**, *60*, 834.
97. K. Kalyanasundaram, *Coord. Chem. Rev.*, **1982**, *46*, 159.
98. J. R. Darwent; K. Kalyanasundaram, *J. Chem. Soc., Faraday Trans. 2*, **1981**, *77*, 373.
99. R. Lomoth; T. Haupl; O. Johansson; L. Hammarström, *Chem. Eur. J.*, **2002**, *8*, 102.
100. E. R. Altwicker, *Chem. Rev.*, **1967**, *67*, 475.

101. Y. Kajii; M. Fujita; H. Hiratsuka; K. Obi; Y. Mori; I. Tanaka, *J. Phys. Chem.*, **1987**, *91*, 2791.
102. I. J. Rhile; T. F. Markle; H. Nagao; A. G. DiPasquale; O. P. Lam; M. A. Lockwood; K. Rotter; J. M. Mayer, *J. Am. Chem. Soc.*, **2006**, *128*, 6075.
103. I. J. Rhile; J. M. Mayer, *Angew. Chem. Int. Ed.*, **2005**, *44*, 1598.
104. A. A. J. Torriero; J. M. Luco; L. Sereno; J. Raba, *Talanta*, **2004**, *62*, 247.
105. D. Evans; J. P. Hart; G. Rees, *The Analyst*, **1991**, *116*, 803.
106. C. Costentin; M. Robert; J.-M. Savéant, *J. Am. Chem. Soc.*, **2006**, *128*, 4552.
107. C. Costentin; M. Robert; J.-M. Savéant, *J. Am. Chem. Soc.*, **2006**, *128*, 8726.
108. C. Costentin; M. Robert; J.-M. Savéant, *J. Am. Chem. Soc.*, **2007**, *129*, 9953.
109. C. J. Fecenko; T. J. Meyer; H. H. Thorp, *J. Am. Chem. Soc.*, **2006**, *128*, 11020.
110. C. J. Fecenko; H. H. Thorp; T. J. Meyer, *J. Am. Chem. Soc.*, **2007**, *129*, 15098.
111. C. Costentin; C. Louault; M. Robert; J.-M. Savéant, *Proc. Natl. Acad. Sci.*, **2009**, *106*, 18143.
112. I. J. Rhile; J. M. Mayer, *J. Am. Chem. Soc.*, **2004**, *126*, 12718.
113. T. F. Markle; I. J. Rhile; A. G. DiPasquale; J. M. Mayer, *Proc. Natl. Acad. Sci.*, **2008**, *105*, 8185.
114. T. F. Markle; J. M. Mayer, *Angew. Chem. Int. Ed.*, **2008**, *47*, 738.
115. S. Y. Reece; D. G. Nocera, *J. Am. Chem. Soc.*, **2005**, *127*, 9448.
116. J. M. Hodgkiss; N. H. Damrauer; S. Presse; J. Rosenthal; D. G. Nocera, *J. Phys. Chem. B*, **2006**, *110*, 18853.
117. L. Biczok; N. Gupta; H. Linschitz, *J. Am. Chem. Soc.*, **1997**, *119*, 12601.
118. A. M. Kuznetsov; J. Ulstrup, *Can. J. Chem.*, **1999**, *77*, 1085.
119. S. Hay; L. O. Johannissen; M. J. Sutcliffe; N. S. Scrutton, *Biophys. J.*, **2010**, *98*, 121.
120. S. Hay; M. J. Sutcliffe; N. S. Scrutton, *Proc. Natl. Acad. Sci.*, **2007**, *104*, 507.
121. L. O. Johannissen; S. Hay; N. S. Scrutton; M. J. Sutcliffe, *J. Phys. Chem. B*, **2007**, *111*, 2631.
122. C. Carra; N. Iordanova; S. Hammes-Schiffer, *J. Am. Chem. Soc.*, **2003**, *125*, 10429.
123. S. Hay; N. S. Scrutton, *Photosynth. Res.*, **2008**, *98*, 169.
124. N. Song; D. M. Stanbury, *Inorg. Chem.*, **2008**, *47*, 11458.
125. M. Sjödin; S. Styring; B. Åkermark; L. Sun; L. Hammarström, *Phil. Trans. R. Soc. Lond. B*, **2002**, *357*, 1471.
126. M. Sjödin; S. Styring; B. Åkermark; L. Sun; L. Hammarström, *J. Am. Chem. Soc.*, **2000**, *122*, 3932.
127. C. Costentin; M. Robert; J.-M. Savéant; A. L. Teillout, *Chem.Phys.Chem.*, **2009**, *10*, 191.
128. C. Costentin; M. Robert; J.-M. Savéant, *J. Am. Chem. Soc.*, **2007**, *129*, 5870.
129. A. Magnuson; H. Berglund; P. Korall; L. Hammarström; B. Åkermark; S. Styring; L. Sun, *J. Am. Chem. Soc.*, **1997**, *119*, 10720.
130. M. Sjödin; S. Styring; H. Wolpher; Y. Xu; L. Sun; L. Hammarström, *J. Am. Chem. Soc.*, **2005**, *127*, 3855.
131. L. I. Krishtalik, *Biochim. Biophys. Acta*, **2003**, *1604*, 13.
132. M. Sjödin; R. Ghanem; T. Polivka; J. Pan; S. Styring; L. Sun; V. Sundström; L. Hammarström, *Phys. Chem. Chem. Phys.*, **2004**, *6*, 4851.
133. C. T. Lin; W. Bottcher; M. Chou; C. Creutz; N. Sutin, *J. Am. Chem. Soc.*, **1976**, *98*, 6536.
134. M. R. Seyedsayamdost; S. Y. Reece; D. G. Nocera; J. Stubbe, *J. Am. Chem. Soc.*, **2006**, *128*, 1569.

Acta Universitatis Upsaliensis

Digital Comprehensive Summaries of Uppsala Dissertations from the Faculty of Science and Technology XXX

Editor: The Dean of the Faculty of Science and Technology

A doctoral dissertation from the Faculty of Science and Technology, Uppsala University, is usually a summary of a number of papers. A few copies of the complete dissertation are kept at major Swedish research libraries, while the summary alone is distributed internationally through the series Digital Comprehensive Summaries of Uppsala Dissertations from the Faculty of Science and Technology. (Prior to January, 2005, the series was published under the title "Comprehensive Summaries of Uppsala Dissertations from the Faculty of Science and Technology".)

Distribution: publications.uu.se
urn:nbn:se:uu:diva-112060

ACTA
UNIVERSITATIS
UPSALIENSIS
UPPSALA
2010